Journal of Statistical Physics, Vol. 95, Nos. 5/6, 1999

Modeling of Phase Separation in Alloys with Coherent Elastic Misfit

Peter Fratzl,[1] Oliver Penrose,[2] and Joel L. Lebowitz[3]

Received October 9, 1998; final March 1, 1999

Elastic interactions arising from a difference of lattice spacing between two coherent phases can have a strong influence on the phase separation (coarsening) behavior of alloys. If the elastic moduli are different in the two phases, the elastic interactions may accelerate, slow down or even stop the phase separation process. If the material is elastically anisotropic, the precipitates can be shaped like plates or needles instead of spheres and can arrange themselves into highly correlated patterns. Tensions or compressions applied externally to the specimen may have a strong effect on the shapes and arrangement of the precipitates. In this paper, we review the main theoretical approaches that have been used to model these effects and we relate them to experimental observations. The theoretical approaches considered are (i) "macroscopic" models treating the two phases as elastic media separated by a sharp interface, (ii) "mesoscopic" models in which the concentration varies continuously across the interface, and (iii) "microscopic" models which use the positions of individual atoms.

KEY WORDS: Kinetics of phase separation; quenched alloys; elastic interactions; sharp interface model; diffuse interface models; atomic lattice models.

Dedicated to John W. Cahn, on the occasion of his 70th birthday.

[1] Erich Schmid Institute of Materials Science, Austrian Academy of Sciences, and University of Leoben, A-8700 Leoben, Austria.

[2] Department of Mathematics, Heriot-Watt University, Riccarton, Edinburgh EH14 4AS, Scotland, U.K.

[3] Departments of Mathematics and Physics, Rutgers University, Hill Center, Busch Campus, New Brunswick, 08903 New Jersey.

0022-4715/99/0600-1429$16.00/0

1. INTRODUCTION

1.1. The Scope of This Paper

The separation of an alloy into two phases is a technologically important phenomenon whose theory owes much to the work of John Cahn. When the two phases first form they are very finely mixed, with a large amount of interface between the two phases. Atoms then diffuse within the material so as to reduce the amount of interface, making the mixture of phases coarser and coarser as time proceeds. The driving force for this coarsening process comes from the free energy of the interface. For many alloys, where the sizes of the two kinds of atoms composing the alloy are not too different, the atoms manage to fit themselves on to a common lattice, but they can achieve this only at the cost of significant distortion of the lattice. At first, the energy arising from this distortion is relatively unimportant, but as the coarsening proceeds the interfacial energy decreases and eventually the elastic interactions, which are of long range and can also be strongly anisotropic, may predominate. This change in the dominant driving force can dramatically affect both the rate of coarsening and the structure of the domains themselves in the late stages of the coarsening process.

In the present article we review some theoretical approaches that have been used to model the effects of elastic interactions on coarsening in alloys. We shall confine ourselves to alloys which are *coherent* (meaning that the lattice structure is only distorted, not disrupted, by the misfit between the two types of atom), and for that reason we shall not consider any effects involving dislocations, such as plasticity. Moreover, we shall consider only first-order phase transformations, in which the concentrations are different in the two phases, so that diffusive transfer of material from one place to another is an essential part of the process; martensitic transformations, for example, will not be considered.

An idea of the relative importance of the elastic and surface energy effects can be obtained by comparing the surface energy of a spherical precipitate of radius R, which is $4\pi\sigma R^2$ where σ is the interfacial energy per unit area (the surface tension), with the elastic energy due to such a precipitate, which is of order $\frac{1}{2}(4\pi R^3/3)\, Gq^2$ where G is a typical elastic modulus, e.g., the shear modulus, and q is a typical strain due to the misfit (see Appendix for symbols). The two energies are equal when $R \sim R_0 = 6\sigma/Gq^2$. At first, the precipitates are much smaller than this size, so that the interfacial tension predominates; but later on in the coarsening process the precipitates will be of this size or larger, so that elastic effects become important. As an example, the value of R_0 for Ni_3Al precipitates in nickel is of order 10^{-7} m, and it has been shown[54] by experiments on a sequence

of alloys with different values for R_0, that some of the effects due to elastic misfit are proportional to R/R_0 at small R/R_0.

We shall describe three different types of model which have been used in the theory of these elastic effects. In the first, the two phases are treated as continuous materials obeying the macroscopic laws of linear elasticity theory[4] and the interface between them is treated as a geometrical surface (i.e., its thickness is ignored). This was the model used by J. D. Eshelby in his pioneering work.[233, 229, 223] We shall call it the sharp interface model. There are two versions of this model: a "static" version in which the energies of different arrangements of the phases are compared without detailed consideration of how the system can get from one arrangement to the other, and a "dynamic" version in which the mechanism for such changes, namely diffusion, is also allowed for. The static version will be considered in Chapter 2 and the dynamic version in Chapter 3.

A second type of model, introduced by John Cahn in 1961, takes the structure of the interface into account by using the concentration of one of the alloy components as a field variable. Such models are sometimes described as "mesoscopic." The concentration field is approximately constant (but at different values) in the two phases, and it varies continuously across the interface. Its time variation is given by a deterministic differential equation, analogous to the Cahn–Hilliard equation.[222] We shall call this the diffuse interface model and describe it in Chapter 4.

In the third type of model a completely microscopic description is used. The atoms are no longer represented by a continuum; instead we follow them individually and model their diffusion by random jumps. Although it gives no analytic results, this method has the merit that the physical assumptions going into it are very simple. It also takes fluctuations into account and therefore includes the possibility of nucleation in a natural way. We shall call it the atomic lattice model and describe it in Chapter 5.

In cases where the lattice parameters are approximately the same in the two phases, so that the elastic misfit is unimportant, all three of these methods have been found to give results in reasonable agreement with experiments. For reviews, see Gunton,[167] Furukawa,[164, 159] Binder.[98] However, when the misfit is important, the theoretical situation becomes more complicated, and it may be that a combination of all the three methods, or more, is necessary for a proper understanding.

Some effects on morphology and kinetics typically observed in experiments are summarized in the next section. Many of these effects are actually

[4] Among the few authors who have looked into possible nonlinear effects are Larché and Cahn[183] and Grinfeld.[151]

reproduced by the various theoretical approaches. These effects range from a change (typically a slowing down) in the rate of precipitate coarsening to a transformation from nearly spherical to cube-like or plate-like precipitates aligned along the elastically soft directions, that is, [100] and equivalent ones in the case of Ni-base alloys. One also observes a direct effect of external stresses on the coarsening behavior of alloys, which can lead to the formation of cylinders or parallel plates with wavy interfaces.

1.2. Experimentally Observed Effects Due to Elastic Misfit Interactions

The aim of the present chapter is not to give an exhaustive review of the effects of elastic misfit strain on the phase separation process but rather to show some typical examples. Because of the huge practical importance of nickel-base superalloys for use at high temperatures, e.g., in turbine blades, these alloys have attracted much interest in recent experimental studies. Most of the following examples will focus on this type of alloy system where the nickel-rich matrix (γ-phase) has a face-centered cubic structure and contains γ'-precipitates with $L1_2$ structure of the type Ni_3X, where X may be Al, Ti, Si, etc.

1.2.1. Morphological Effects. Depending on the composition of the alloy, the precipitates may be either round as, e.g., in Ni-Al-Si[68] or cube-like as in, for example, Ni-Al.[79] The cube-like shape is, in fact, very frequent in this type of system, appearing also in ternary alloys like Ni-Al-Mo,[120, 112, 57, 58, 46, 24] Ni-Al-Ti[125] or Ni-Al-Cr.[132] The generally accepted reason for the cube-like shape is the effect of anisotropic elasticity. A further observation is the alignment of these precipitates, like strings of pearls, along the elastically soft directions.

As an example, we show in Fig. 1 typical transmission electron microscopy (TEM) and small-angle X-ray scattering (SAXS) data for Ni-Al-Mo alloys. This ternary alloy system has the property that the lattice misfit depends on the molybdenum content in such a way that negative, positive or zero misfit is possible.[120] Figure 1a shows the TEM data for an alloy with no misfit. The γ' precipitates, which appear white, are round in this case, and arranged at random. The SAXS pattern (Fig. 1b), which represents roughly the square of the Fourier transform of the microstructure (as depicted in Fig. 1a), is completely isotropic. This symmetry shows that there is no preferred direction in the configuration of the particles. This situation is exactly what one expects for a precipitate microstructure which coarsens to reduce the total amount of interface between matrix and precipitates.

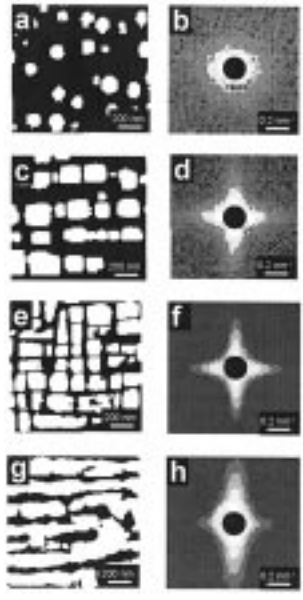

Fig. 1. (a) Transmission electron micrograph (TEM) of Ni-Al-Mo alloy with Mo-composition chosen such as to make the lattice spacing in matrix and precipitates (gamma-prime phase) equal. Treatment: 430 h at 1048 K after quench from the single-phase region. The plane of observation corresponds to the crystallographic plane (001). One observes round precipitates i.e., no elastic effects. (b) Small-angle X-ray scattering (SAXS) data from the same specimen in the same orientation. One observes an isotropic scattering pattern. (c) TEM of the (001)-plane of a Ni-Al-Mo alloy with Mo-composition chosen such as to make the lattice spacing in the precipitates (gamma-prime phase) larger by 0.4%. Same thermal treatment as in (a). One observes cube-like precipitates, aligned along the elastically soft directions, [010] and [100]. (d) SAXS from the Specimen in (c). There is a flower-like pattern with four-fold symmetry, the elongations being in [010] and [100]-directions (indicating flat interfaces and strong correlations in those directions). (e) TEM of Ni-Al-Mo alloy with Mo-composition chosen such as to make the lattice spacing in the precipitates (gamma-prime phase) smaller (misfit -0.5%). Treatment: 5 h at 1253 K (Orientation 001). The patterns are qualitatively similar to those in (c). (f) SAXS from the specimen in (e). (g) Same alloy and heat-treatment as in (e), but now with an external compressive load of 130MPa applied to it along the vertical [010]-direction. (h) SAXS from the specimen in (g). Note that the horizontal streak has disappeared, corresponding to the disappearence of vertically oriented interfaces in (g). The data in (a)–(d) are taken from ref. 46 and in (e)–(h) from ref. 24.

For comparison, Figs. 1c and 1d show the corresponding data for a Ni-Al-Mo alloy with similar fraction of γ' phase but where the molybdenum content was adjusted to give a lattice misfit. Now the precipitates are cube-like rather than spherical and they are arranged like strings of pearls along the cubic directions [100] or equivalent ones. Correspondingly, the SAXS patterns are no longer spherically symmetric, although they still

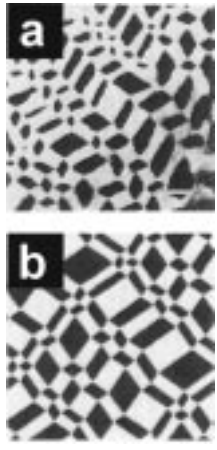

Fig. 2. (a) Chessboard-like microstructure observed by transmission electron microscopy in $Co_{39.5}$-$Pt_{60.5}$ slowly cooled from 1023 K and aged 15 days at 873 K. The scale bar represents 30 nm. The cubic phase appears white while the tetragonal phase is black. (b) Computer simulation using a diffuse interface model (From ref. 1).

have cubic symmetry. Figure 1e and Fig. 1f show a similar situation but with a higher volume fraction of γ' precipitates. Strongly periodic arrangements of precipitates are also found in alloys like Ti-Ni.[113, 28]

In some other types of alloys, a typical example being Al-Cu[22] it is also common to find plate-like coherent precipitates as a result of elastic misfit strains. The example of the so-called "Guinier-Preston zones" in Al-Cu is particularly striking, since these coherent precipitates are practically monoatomic layers of copper which create large elastic distortions in the aluminium matrix. Other examples of alloys with plate-like precipitates are Cu-Be[48] and internally oxidized Cu-Fe.[69, 65]

A striking effect has been observed in alloys of the type Co-Pt[103] or (CuAu)-Pt[59] where precipitates with tetragonal structure are developing in a cubic matrix. Figure 2a (from ref. 1) shows the tile-like structures that can develop.

Finally, it has been found in some nickel-base alloys that large cube-like precipitates may even split into several smaller ones[71, 163] a process which has also been related to elastic interactions[141] (see Fig. 4).

1.2.2. Effects on Coarsening Kinetics. The reported effects on the rate of coarsening are seemingly less consistent. In some cases, an increase of the mean precipitate radius proportional to $t^{1/3}$, t being the annealing time, has been reported, as in Ni-Al-Mo[112, 46] or Ni-Al-Si.[68]

This growth law is very similar to what is usually found in alloys without lattice misfits and in computer simulations. It is due to a ripening process, described in the Lifshitz–Slyozov–Wagner (LSW) theory,[225, 226] where the large precipitates grow at the expense of the small ones, thereby reducing the total interface area between matrix and precipitates.

In some other cases, e.g., Ni-Cu-Si alloys, the coarsening starts out according to a $t^{1/3}$ but slows down in later stages, eventually even coming to a standstill. This behaviour is illustrated in Fig. 3 where the growth of the mean precipitate size R is plotted for Ni-Al-Mo (Fig. 3a) and for Ni-Cu-Si (Fig. 3b) alloys. Another example of this type of behaviour is provided by the titanium-rich ω-phase precipitates in Ti-Mo[67] (see Fig. 3c). (A slowing down of coarsening had also been reported early on for the binary alloy Ni-Si where the misfit is rather small,[132] but this was not confirmed in later studies.[17]) The usual interpretation of this slowing down is *inverse coarsening*, which means that, because of the elastic interaction, smaller precipitates may grow at the expense of larger ones even though this increases the interfacial area.

There is, however, no generally accepted explanation for the fact that slowing down of coarsening is observed in some cases but not in all. One possibility is that the inverse coarsening may reduce the prefactor λ in the expression

$$R \approx \lambda t^{1/3} \tag{1}$$

instead of affecting the exponent 1/3. This is, indeed, observed in some Ni-Al-Si alloys[68] Another proposal is that there could be an interplay between elastic heterogeneity and anisotropy such that inverse coarsening would only become predominant in cases where the anisotropy is not too large.[55, 30]

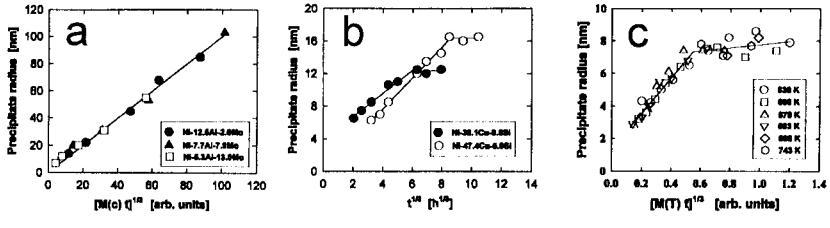

Fig. 3. Time-dependence of the mean precipitate size for (a) Ni-Al-Mo alloys (from ref. 46), (b) Ni-Cu-Si alloys (from ref. 149) and (c) Ti-Mo alloys (from ref. 67). The coefficients $M(c)$ in (a) and $M(T)$ in (c) are used to scale data obtained for different alloy compositions or different temperatures, respectively.

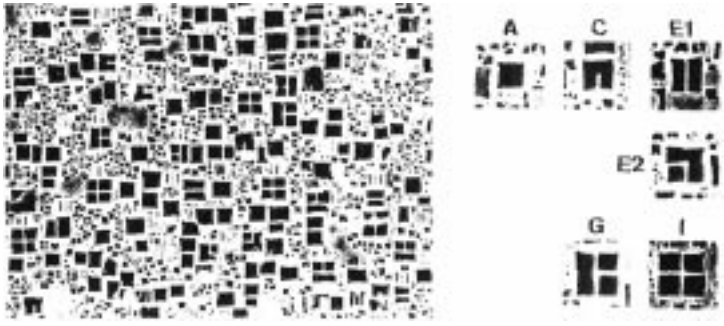

Fig. 4. Typical example of ordered precipitates in a nickel-base superalloy, which split into several pieces during the coarsening process (from ref. 71).

1.2.3. The Role of Applied Stress; Rafting. When an external stress is applied to an alloy it can cause the shapes and arrangement of the precipitates to change. For example, as already mentioned and shown in Fig. 1c–f, in a nickel-base alloy annealed without external stress the precipitates are approximately cubes and are arranged in a cubic array, in conformity with the cubic symmetry of the crystal. If a compression is applied along the [010] axis the precipitates shorten along this axis and widen along the other two axes. At large enough compression the precipitates join up and form plates at right angles to the [010] direction. On the other hand a tension along the [010] axis causes the precipitates to lengthen along this axis and eventually form rods. This behaviour is shown for the case of the Ni-Al-Mo alloy system in Fig. 1g. The corresponding SAXS pattern (Fig. 1h) shows clearly the breaking of the cubic symmetry. Pictures very similar to Fig. 1h have been published very recently for a uniaxially strained commercial nickel-base superalloy studied by small-angle neutron scattering.[27]

This phenomenon, known as rafting, was first observed experimentally by Webster and Sullivan,[213] Sullivan *et al.*[210] and Tien and Copley.[202] A well-written short review of the subject is given in ref. 36; see also ref. 38. The mechanism of rafting is thought by many authors (Socrate and Parks 1993,[82] Pollock and Argon 1994,[70] Vallés and Arrell 1994,[64, 74] Buffière and Ignat 1995,[44] Svoboda and Lukáč,[41] Ohashi *et al.* 1997[23]) to involve not only the diffusional and elastic effects considered here but also dislocations and plasticity; however such considerations are beyond the scope of this paper.

2. THE STATIC SHARP INTERFACE MODEL

In the sharp interface model the two phases, which we call α and β, are modelled as distinct regions of space which, together with the sharp interface between them, make up the entire region Ω occupied by the specimen. The two regions will be called Ω^α and Ω^β, and the interface between them will be denoted by Γ. It frequently happens that one of the phases consists of disconnected domains called precipitates or inclusions, while the other phase, called the matrix, occupies the remaining region which looks something like a Swiss cheese. In this case we shall normally take Ω^α to comprise the inclusions and Ω^β to be the matrix.

There are two versions of the sharp-interface model, which we shall call the static and dynamic versions. In the static version, time evolution is not considered, and the local composition of the alloy need not be considered either; the main thing that the model can do is to compare the (free) energies of various configurations of inclusions. In the dynamic version, which we shall consider in the next chapeter, we do consider time evolution, and since the mechanism for time evolution is diffusion the local composition of the alloy must then be included in the model.

Although the static model contains no explicit time evolution and therefore no coarsening, it does provide information about time evolution and coarsening through the principle that the free energy must decrease with time. For example, we can look for the energy-minimizing shape of an isolated inclusion of a given volume, and under suitable conditions the actual inclusions having this volume should be close to this shape (which is not necessarily spherical, even in an isotropic material). The theory of the model also contains important general results about the elastic energy, such as the "Bitter-Crum" theorem (see Section 2.1.4), and the elasticity theory contained in it underpins the models described in later sections.

2.1. Theory of the Energy of Inclusions in an Elastic Medium

The free energy of the system can be written in the form

$$F = \int_\Omega (f + w)\, \mathrm{d}^3\mathbf{x} + F^\Gamma + W^{ext} \tag{2}$$

where f denotes the thermodynamic free energy density at zero macroscopic stress, w is the elastic free energy density (defined as the additional free energy density due to the macroscopic stress), F^Γ denotes the free energy of the interface and W^{ext} denotes the potential energy of any external mechanism that the specimen may be connected to, for example a weight

attached to one end of the specimen. In the static version of the model, which we are considering in this chapter, the value of f can be different in the two phases, but is uniform throughout each phase. The variable of integration $\mathbf{x}$ is the coordinate of the relevant material point in the unstrained reference state of the material, so that a given material point always has the same value of $\mathbf{x}$, regardless of where the deformation has taken it to.

To write down a formula for the elastic energy density w we first define the *displacement field* $\mathbf{u}$; its definition is that the material point $\mathbf{x}$ in the undeformed material[5] will be found at the point $\mathbf{x}+\mathbf{u}(\mathbf{x})$ in the deformed material. The *strain tensor* is then defined (we are using linear elasticity theory; for the nonlinear formula see Eqs. (1), (3) of ref. 228) by giving its Cartesian components[6]

$$e_{ij}(\mathbf{x}) = \frac{1}{2}\left(\frac{\partial u_i}{\partial x_j} + \frac{\partial u_j}{\partial x_i}\right) \tag{3}$$

We shall also need the *stress-free strain* tensor[7] $e^0_{ij}(\mathbf{x})$, defined as the value which the strain tensor at $\mathbf{x}$ would have if the material were uniform and unstressed. The stress-free strain is taken to be a different constant in each of the two phases, corresponding to their different chemical compositions. The difference between the stress-free strains in the two phases is called the *transformation strain* or *misfit strain*. A common assumption is that, under zero stress, one of the two phases is simply a scaled-up version of the other. Let us denote the scale factor by $1+q$, so that the stress-free lattice spacing of the inclusion material is greater than that of the matrix material by a factor $1+q$, corresponding to a relative difference in specific volume of approximately $3q$ if q is small. Then the stress-free strain can be given the

[5] There is some arbitrariness in the choice of an "undeformed" lattice, since a uniform expansion of an undeformed lattice gives another undeformed lattice. Different choices of undeformed lattice are related by a dilatation of the coordinate system, which adds the same constant multiple of the unit tensor to $\partial u_i/\partial x_j$ and to the stress-free strain tensor. This transformation leaves the energy expression (5) invariant or (if the externally applied stress, modelled as in Eq. (9), includes an isotropic component) merely adds to it a constant which is independent of the state of the specimen. Physically measurable quantities such as the energy differences between different configurations and the differences of the stress-free strains between the two phases are not affected by the choice of undeformed lattice.

[6] Some authors omit the factor 1/2 in Eq. (3) when $i \neq j$, but if that is done then e_{ij} is not a tensor.

[7] This tensor has also been called the "intrinsic strain",[160] and the "spontaneous deformation".[156] It is an example of what Mura[175] calls an "eigenstrain."

value zero in the matrix (this corresponds to a particular choice for the reference state of the material) and to have the simple form

$$e^0_{ij} = q\delta_{ij} \tag{4}$$

in the inclusions.

In linear elasticity the elastic energy is a quadratic function of the strain tensor. In view of our convention that the elastic energy is zero at zero stress, we can write this quadratic function

$$w = \tfrac{1}{2} \sum_{ijmn} \lambda_{ijmn}(e_{ij}(\mathbf{x}) - e^0_{ij}(\mathbf{x}))(e_{mn}(\mathbf{x}) - e^0_{mn}(\mathbf{x})) \tag{5}$$

Here λ_{ijmn}, a fourth-rank tensor, is called the (isothermal) *elasticity tensor* or *stiffness tensor*. This tensor is positive definite, in the sense that w is positive unless the tensors e_{ij} and e^0_{ij} are equal. In principle the components λ_{ijmn} depend on the local chemical composition and therefore on position, but in the static sharp-interface model this dependence is generally neglected and the λ_{ijmn} are taken to be constant in each phase, though not necessarily the same constant. Likewise, the stress-free strain tensor e^0_{ij} is generally taken to be a constant in each phase (as in the example given above, Eq. (4)), though its dependence on composition has been taken into account in some calculations, for example ref. 153.

The formula (5), which generalizes a standard formula of elasticity theory (Eqs. (10), (1) of ref. 228) to the case of non-vanishing stress-free strains, has been in use in one form or another since the beginnings of this subject (e.g., refs. 223, 215, 212). It corresponds to a particular way of apportioning the total free energy density between the two terms f and w, in which f is defined to be the free energy at zero stress. The alternative convention, to define f as the free energy at zero strain, has also been used.[116]

The λ_{ijmn}'s are symmetric under interchange of i and j, of m and n, and of the pair (i, j) with the pair (m, n); and they usually have further symmetries reflecting the symmetries of the crystal lattice. The most symmetrical case of all is an isotropic solid such as rubber, for which the elastic energy density simplifies (in linear elasticity theory) to

$$w = \tfrac{1}{2}K\left\{\sum_k (\Delta e)_{kk}\right\}^2 + G\sum_{ij}\left\{(\Delta e)_{ij} - \tfrac{1}{3}\delta_{ij}\sum_k (\Delta e)_{kk}\right\}^2 \tag{6}$$

where K is the *bulk modulus*, $(\Delta e)_{ij}$ means $e_{ij} - e^0_{ij}$, G is the *shear modulus* (often denoted by μ) and $\sum_{ij}$ means $\sum_i \sum_j$. The non-zero elements of the elasticity tensor in this case are $\lambda_{1111} = K + \frac{4}{3}G$, $\lambda_{1122} = K - \frac{2}{3}G$, $\lambda_{2323} = G$

and the ones related to these by symmetry, e.g., $\lambda_{1221} = \lambda_{2323}$. A more realistic case for metallurgists is the cubic crystal, for which in the conventional notation

$$w = \tfrac{1}{2}C_{11}\sum_i (\Delta e)_{ii}^2 + C_{12}\{(\Delta e)_{11}(\Delta e)_{22} + (\Delta e)_{22}(\Delta e)_{33} + (\Delta e)_{33}(\Delta e)_{11}\} + 2C_{44}((\Delta e)_{12}^2 + (\Delta e)_{23}^2 + (\Delta e)_{31}^2) \tag{7}$$

so that $\lambda_{1111} = C_{11}$, $\lambda_{1122} = C_{12}$, $\lambda_{2323} = C_{44}$, etc.

For the interfacial energy term F^{Γ} in (2) we shall use the simplest reasonable assumption,

$$F^{\Gamma} = \sigma\,|\Gamma| \tag{8}$$

where σ is the surface tension, assumed constant, and $|\Gamma| = \int_{\Gamma} \mathrm{d}^2\mathbf{x}$ denotes the area of the *undeformed* interface. More general possibilities have also been considered—anisotropic surface energy by Cahn and Hoffman (1974),[193] surface energy depending on the deformation as well as the undeformed area by Gurtin and Murdoch (1975),[191] Cahn and Larché (1982)[172]—but these refinements have not been important in the theory of coarsening.

To model the externally applied forces in a simple way, we shall assume that there are no body forces, and that the tractions (forces per unit area) applied to the surface $\partial\Omega$ of the specimen are of the form $\sum_j t_{ij}^{ext} n_j$, where n_j is the unit outward normal vector and t_{ij}^{ext}, which we take to be symmetric and independent of position, is the *externally applied stress* tensor. The energy W^{ext} of the mechanism providing these tractions can then be equated to its energy when the specimen is in the reference state minus the work it does in bringing the specimen from its reference state to the state with displacement field u_i, so that

$$W^{ext} = \text{const.} - \int_{\partial\Omega} \sum_{ij} u_i t_{ij}^{ext} n_j \,\mathrm{d}^2\mathbf{x} \tag{9}$$

Choosing the constant to be zero, and using first the divergence theorem (applied to the vector field obtained by multiplying u_i by a unit vector in the j direction) and then the formula (3) and the symmetry of t_{ij}^{ext} we can write this in the alternative form

$$W^{ext} = -\int_{\Omega} \sum_{ij} t_{ij}^{ext} \frac{\partial u_i}{\partial x_j} \,\mathrm{d}^3\mathbf{x} = -\int_{\Omega} \sum_{ij} t_{ij}^{ext} e_{ij} \,\mathrm{d}^3\mathbf{x} \tag{10}$$

In this formula, e_{ij} is the strain in the presence of the externally applied stress, which in linear elasticity is an affine function[8] of t_{ij}^{ext}. To first order in the externally applied stress, therefore, the strain e_{ij} in (10) can be given the value it has when there is no externally applied stress.

2.1.1. Elastic Equilibrium. To evaluate the elastic terms in (2), we need the displacement u_i at each point in space. The condition determining u_i is that it should minimize the elastic energy $\int_\Omega w \, d^3\mathbf{x} + W^{ext}$. The Euler–Lagrange equation for this minimization, called the *equation of elastic equilibrium* (Eqs. (2), (6) of ref. 228), is (since t_{ij}^{ext} is a constant)

$$\sum_j \frac{\partial t_{ij}}{\partial x_j} = 0 \tag{11}$$

where t_{ij} is the stress tensor, defined (Eqs. (3), (6) of ref. 228) by

$$t_{ij} = \frac{\partial w}{\partial u_{i,j}} \tag{12}$$

in which $u_{i,j}$ means $\partial u_i / \partial x_j$.

Using (5) in (12) we find with the help of the symmetry relation $\lambda_{ijmn} = \lambda_{jimn}$ that the stress tensor is related to the strain tensor by

$$t_{ij} = \sum_{mn} \lambda_{ijmn}(e_{mn} - e_{mn}^0) \tag{13}$$

(Hooke's law) and is therefore symmetric. In the isotropic case, with w given by (6), Hooke's law takes the form

$$t_{ij} = K\delta_{ij} \sum_k (\Delta e)_{kk} + 2G \left\{ (\Delta e)_{ij} - \tfrac{1}{3}\delta_{ij} \sum_k (\Delta e)_{kk} \right\} \tag{14}$$

To complete the specification of the elastic equilibrium problem, we need conditions on the elastic field variables at the interface Γ and at the boundary of the specimen. On Γ, the condition of coherence requires $\mathbf{u}$ to be continuous:

$$[\mathbf{u}] = 0 \tag{15}$$

where $[\mathbf{u}]$ means $[\mathbf{u}]_\beta^\alpha$, that is $\mathbf{u}^\alpha - \mathbf{u}^\beta$, the difference between the limiting values of $\mathbf{u}$ on the two sides of the interface. Moreover, the values taken by the field $\mathbf{u}$ at the interface (which describe the position of the interface in

[8] That is, a constant plus a linear function.

the deformed material) must satisfy an energy minimization condition. Since we are assuming that the energy of the interface depends only on its position relative to the lattice, the surface energy is not changed by changes of the value of **u** at the interface, and minimization of the elastic energy gives the condition

$$\sum_j [t_{ij}]\, n_j = 0 \tag{16}$$

where $[t_{ij}]$ means $t_{ij}^{\alpha} - t_{ij}^{\beta}$, and **n** is a vector normal to the interface. The physical interpretation of Eq. (16) is that the forces exerted on the interface by the material on each side of it must be equal and opposite.[9]

The boundary conditions at the surface of the specimen depend on the physical situation there. If the boundary of the specimen is clamped, then the system of Eqs. (11) and (13) should be solved subject to prescribed values of u_i on $\partial\Omega$. In the more common situation where known forces are applied at the boundary the boundary condition (analogous to (16) and obtained by minimizing F without restricting u_i at the boundary) is that the surface tractions due to the internal stresses are equal to the externally applied surface tractions:

$$\sum_j t_{ij} n_j = \sum_j t_{ij}^{ext} n_j \tag{17}$$

where, as before, n_j denotes a unit vector normal to the boundary $\partial\Omega$.

It is also possible to use periodic boundary conditions, taking Ω to be a cube (or rectangular prism) and requiring the stress and strain fields to be periodic with unit cell Ω. (Periodic boundary conditions rule out the consideration of surface effects, of course, but such effects do not concern us here.) In general, the displacement field u_i will not be periodic, but by virtue of (3) it can be written in the form

$$u_i = u_i' + \sum_j U_{ij} x_j \tag{18}$$

where u_i' is periodic[10] and U_{ij} is a constant tensor, not necessarily symmetric. Then, using (3), the strain can be written in the manifestly periodic form

$$e_{ij} = \bar{e}_{ij} + \frac{1}{2}\left(\frac{\partial u_i'}{\partial x_j} + \frac{\partial u_j'}{\partial x_i}\right) \tag{19}$$

[9] If the interfacial energy depends on the deformations as well, then an extra term appears in (16); see Gurtin and Murdoch (1975),[191] Cahn and Larché (1982).[172]

[10] Khachaturyan[170] calls u_i' the "local displacement."

where the constant tensor $\bar{e}_{ij}$ is the space-averaged strain

$$\bar{e}_{ij} = \frac{1}{|\Omega|} \int_{\Omega} e_{ij}(\mathbf{x})\, \mathrm{d}^3\mathbf{x} = \frac{1}{2}(U_{ij} + U_{ji}) \tag{20}$$

The value of $\bar{e}_{ij}$ does not appear in the elastic equilibrium equations but it can be determined by direct minimization of F (as given by (2) after using (19) in (5) and (10)) with respect to $\bar{e}_{ij}$; the minimum occurs when

$$\int_{\Omega} t_{ij}\, \mathrm{d}^3\mathbf{x} = \int_{\Omega} t_{ij}^{ext}\, \mathrm{d}^3\mathbf{x} \tag{21}$$

(The transformation (19) is also useful for the case where **u** is fixed at the boundary, since one may be able to make **u** zero on the boundary by a suitable choice of U_{ij}.)

2.1.2. The Interface Condition for Inclusions of Fixed Volume. In the static sharp-interface model, we are only concerned with equilibrium configurations, not in how they are reached. Since diffusion is being neglected, the amount of solute in each inclusion cannot change, and since the concentration in each phase is also fixed, the volume of the inclusion cannot change. In this model, therefore, the shapes and positions of the surfaces Γ surrounding each inclusion are to be found by minimizing the energy subject to the constraint that the volume of each precipitate is held fixed. In this section we formulate a necessary condition which Γ must satisfy at any such energy minimum.

Let Γ be the surface of an inclusion Ω^α in a matrix Ω^β and consider a small displacement of Γ to a new position Γ', each point $\mathbf{x}$ on Γ moving to point $\mathbf{x} + \mathbf{n}(\mathbf{x})\, \delta x(\mathbf{x})$ on Γ' (see Fig. 5). Here $\mathbf{n}(\mathbf{x})$ is a unit vector perpendicular to Γ at $\mathbf{x}$, pointing outwards from the inclusion (i.e., from Ω^α to Ω^β, and $\delta x(\mathbf{x})$, a small scalar, is the signed perpendicular distance from $\mathbf{x}$ to the nearest point on Γ', positive if this point is in the β phase of the Γ configuration. Denote the region between Γ and Γ' by $\delta\Omega^\alpha$. Since we are not considering diffusion at present, the volume of the inclusion is fixed, so that the volume of $\delta\Omega^\alpha$, with an appropriate sign convention, is zero. Thus we have (to lowest order in δx)

$$\int_{\Gamma} \delta x\, \mathrm{d}^2\mathbf{x} = 0 \tag{22}$$

Now consider the change in energy on going from Γ to Γ'. There is no change in the total thermodynamic free energy $\int f\, \mathrm{d}^3\mathbf{x}$, since the volume of the inclusion does not change. The change (increase) in the elastic energy

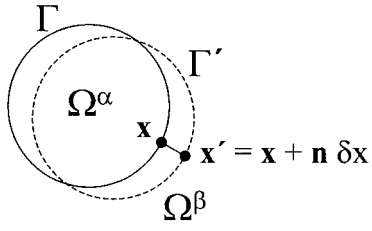

Fig. 5. Geometrical objects used in Section 2.1.2.

between the two configurations, as given by Eq. (2), is the sum of three terms:

1. the change in surface energy due to the change in the area of Γ. This energy increase is equal (in three dimensions) to the surface tension σ times the increase in undeformed area $\int_\Gamma (2\kappa\,\delta x)\,\mathrm{d}^2\mathbf{x}$, where κ is the mean curvature, taken positive if the centre of curvature is on the α side of Γ.

2. the change in total elastic energy due to the fact that (for positive δx) the region $\delta\Omega^\alpha$, which was previously on the β side of the interface, is now on the α side. To lowest order in δx this increase is $\int_\Gamma [w]\,\delta x\,\mathrm{d}^2\mathbf{x}$ where $[w] = w^\alpha - w^\beta$ is the difference between the elastic energy densities on the two sides of the interface at $\mathbf{x}$.

3. The change in the elastic energy due to changes $\delta\mathbf{u}$ in the displacement field outside $\delta\Omega^\alpha$. Denoting these displacements by $\delta\mathbf{u}$ and using the definition (12) of t_{ij} we can write the energy change, to lowest order, as

$$\int_\Omega \sum_{ij} t_{ij}\,\delta u_{i,j}\,\mathrm{d}^3\mathbf{x} = \int_\Omega \sum_{ij} \{(t_{ij}\,\delta u_i)_{,j} - t_{ij,j}\,\delta u_i\}\,\mathrm{d}^3\mathbf{x} \tag{23}$$

where the notation $(\cdots)_{,j}$ means $\partial(\cdots)/\partial x_j$. The second term in the integrand is zero because of the elastic equilibrium condition (11). Applying the divergence theorem separately to the regions Ω^α and Ω^β, and assuming that the surface of the specimen is either held fixed, so that $\delta\mathbf{u} = 0$ there, or is too far away to matter, we can simplify the remaining term to

$$\int_\Gamma \sum_{ij} n_j [t_{ij}\,\delta u_i]\,\mathrm{d}^2\mathbf{x} = \int_\Gamma \sum_{ij} n_j t_{ij}^\alpha [\delta u_i]\,\mathrm{d}^2\mathbf{x} \tag{24}$$

by (16). The last equation would also be true with t_{ij}^β replacing t_{ij}^α. To evaluate $[\delta u_i]$ (which means $[\delta u_i]_\beta^\alpha$) we write it as a line integral across $\delta\Omega^\alpha$

$$[\delta u_i] = [\delta u_i]^{\alpha}_{\beta} = -[\delta u_i]^{\beta}_{\alpha} = -\int_0^{\delta x} \sum_j \frac{\partial(\delta u_i)}{\partial x_j} n_j \, dz$$

$$= -\int_0^{\delta x} \sum_j \delta \frac{\partial u_i}{\partial x_j} n_j \, dz$$

$$= -\delta x \sum_j [u_{i,j}] \, n_j \tag{25}$$

Adding together the three contributions we find for the change in the total energy W

$$\delta W = \int_{\Gamma} \left\{ 2\sigma\kappa + [w] - \sum_{ik} T_i [u_{i,k}] \, n_k \right\} \delta x \, d^2\mathbf{x} \tag{26}$$

where we have defined $T_i = \sum_j t^{\alpha}_{ij} n_j = \sum_j t^{\beta}_{ij} n_j$, the normal traction at the interface.

For W to be a minimum against arbitrary changes of shape or position of the inclusion which satisfy the constant-volume condition (22) it is necessary for the coefficient of δx in the integrand of (26) to satisfy

$$2\sigma\kappa + [w] - \sum_{ik} T_i [u_{i,k}] \, n_k = p \tag{27}$$

where p is a Lagrange multiplier, the same at all points on Γ, which can be thought of as the excess pressure inside the inclusion. If there is more than one inclusion, p can be different for different inclusions.

If the inclusion is not in equilibrium with respect to changes of shape or position, then its surface will tend to move, since the energy can be decreased by moving the interface towards the α phase in the places where the left side is greater than the right side, and towards the β phase in the places where the right side is greater. The mechanism for this movement of the interface is diffusion, which we discuss in Chapter 3.

2.1.3. The Fourier Transform Solution. If the elasticity tensor is independent of position (i.e., for the sharp interface model, if it is the same in both phases) we speak of *homogeneous elasticity*. In that case, the equation of elastic equilibrium, (11), can be solved by Fourier transforms for the case where Ω is a rectangular box with periodic boundary conditions. In this way the elastic energy of an arbitrary arrangement of inclusions in such a box, or an arbitrary periodic arrangement of inclusions in an infinite specimen, can be expressed as a sum or integral in Fourier space. Moreover, the stress-free strain tensor e^0_{ij} need not be restricted to two different values, one in Ω^{α} and the other in Ω^{β}, but can vary with

position in any way. This method of solution has been extensively developed by Khachaturyan[215, 209, 170] and by Mura.[175]

We define the Fourier components of the displacement vector and the stress-free strain tensor by

$$\tilde{\mathbf{u}}(\mathbf{k}) = \int_{\Omega} e^{i\mathbf{k}\cdot\mathbf{x}} \mathbf{u}'(\mathbf{x})\, d^3\mathbf{x} \tag{28}$$

$$\tilde{e}^0_{ij}(\mathbf{k}) = \int_{\Omega} e^{i\mathbf{k}\cdot\mathbf{x}} e^0_{ij}(\mathbf{x})\, d^3\mathbf{x} \tag{29}$$

where $\mathbf{u}'$ is the vector whose components u'_i are defined in (18). Using Parseval's theorem and the symmetries such as $\lambda_{ijmn} = \lambda_{jimn}$, the elastic energy formula implied by (5) and (10) can be written

$$\begin{aligned} W(e_{ij}(\cdot)) &= \int_{\Omega} \left(w - \sum_{ij} t^{ext}_{ij} e_{ij} \right) d^3\mathbf{x} \\ &= \frac{1}{2\,|\Omega|} \sum_{\mathbf{k}\neq 0} \sum_{ijmn} (i\tilde{u}^*_i(\mathbf{k})\, k_j - \tilde{e}^0_{ij}(\mathbf{k}))\, \lambda_{ijmn}(-i\tilde{u}^*_m(\mathbf{k})\, k_n - \tilde{e}^0_{mn}(\mathbf{k})^*) \\ &\quad + \frac{|\Omega|}{2} \sum_{ijmn} (\bar{e}_{ij} - \bar{e}^0_{ij})\, \lambda_{ijmn} (\bar{e}_{mn} - \bar{e}^0_{mn}) - |\Omega| \sum_{ij} t^{ext}_{ij} \bar{e}_{ij} \end{aligned} \tag{30}$$

where $|\Omega|$ means the volume of Ω, the star denotes a complex conjugate, the $\mathbf{k}$-summation goes over the reciprocal lattice of Ω, $\bar{e}_{ij}$ means the space average of $e_{ij}(\mathbf{x})$ (see Eq. (20)) and $\bar{e}^0_{ij}$ means the space average of e^0_{ij}. Minimizing the right side of (30) with respect to $\mathbf{u}(\mathbf{k})$ and $\bar{e}_{ij}$, we obtain for the actual elastic energy (see refs. 215, 208, 170)

$$W = \frac{1}{2\,|\Omega|} \sum_{\mathbf{k}\neq 0} \sum_{ijmn} \tilde{e}^0_{ij}(\mathbf{k})^*\, \Psi_{ijmn}(\mathbf{k})\, \tilde{e}^0_{mn}(\mathbf{k}) - |\Omega| \sum_{ij} t^{ext}_{ij} \left(\bar{e}^0_{ij} + \frac{1}{2} e^{ext}_{ij} \right) \tag{31}$$

where

$$\Psi_{ijmn}(\mathbf{k}) = \lambda_{ijmn} - \sum_{pqrs} \lambda_{ijpq} k_p Z_{qr}(\mathbf{k})\, k_s \lambda_{rsmn} \qquad (\mathbf{k}\neq 0) \tag{32}$$

$Z_{ij}(\mathbf{k})$ being the inverse of the matrix

$$(Z^{-1})_{ij} = \sum_{mn} k_m \lambda_{imnj} k_n \tag{33}$$

and e^{ext}_{ij} means the solution of $\sum_{mn} \lambda_{ijmn} e^{ext}_{mn} = t^{ext}_{mn}$. Note that Ψ_{ijmn} is homogeneous of degree zero in $\mathbf{k}$: it depends only on the direction of the vector $\mathbf{k}$, not on its length. Also, $\Psi(\mathbf{k})$ is positive semi-definite for each

value of $\mathbf{k}$, in the sense that $\sum_{ijmn} e_{ij}^* \Psi_{ijmn}(\mathbf{k})\, e_{mn} \geqslant 0$ for any tensor e_{ij}; this property follows from the fact that this last sum is the value of the obviously positive corresponding term of the sum over $\mathbf{k}$ in (30) for a particular value of $\mathbf{u}(\mathbf{k})$.

In an alloy where $e_{ij}^0(\mathbf{x})$ takes just two values, e_{ij}^α in Ω^α and e_{ij}^β in Ω^β, the definition (29) gives

$$\tilde{e}_{ij}^0(\mathbf{k}) = [e_{ij}^0]\, \theta(\mathbf{k}) \qquad (\mathbf{k} \neq 0) \tag{34}$$

where $[e_{ij}^0]$ stands for the transformation strain $e_{ij}^\alpha - e_{ij}^\beta$ and $\theta(\mathbf{k})$ is defined by

$$\theta(\mathbf{k}) = \int_{\Omega^\alpha} \mathrm{e}^{\mathrm{i}\mathbf{k}\cdot\mathbf{x}}\, \mathrm{d}^3\mathbf{x} \tag{35}$$

Substitution of (34) into (31) gives Khachaturyan's formula[215, 170]

$$W - W^{ext} = \tfrac{1}{2} \sum_{\mathbf{k}\neq 0} B(\mathbf{k})\, |\theta(\mathbf{k})|^2 \tag{36}$$

where we define

$$B(\mathbf{k}) = \sum_{ijmn} [e_{ij}^0]\, \Psi_{ijmn} [e_{mn}^0] \tag{37}$$

Like $\Psi_{ijmn}(\mathbf{k})$, the function B depends only on the direction of the vector $\mathbf{k}$, not on its length.

Using Parseval's theorem, the sum over $\mathbf{k}$ in (31) can be expressed as an integral over position space:

$$W = \frac{1}{2\,|\Omega|} \iint_\Omega \sum_{ijmn} (e_{ij}^0(\mathbf{x}) - \bar{e}_{ij}^0)\, H_{ijmn}(\mathbf{x}-\mathbf{y})(e_{mn}^0(\mathbf{y}) - \bar{e}_{mn}^0)\, \mathrm{d}^3\mathbf{x}\, \mathrm{d}^3\mathbf{y} + W^{ext} \tag{38}$$

where H_{ijmn} stands for $|\Omega|^{-1} \sum_{\mathbf{k}\neq 0} \Psi_{ijmn}(\mathbf{k})\, e^{-i\mathbf{k}\cdot\mathbf{x}}$, the inverse Fourier transform of Ψ_{ijmn}, and W^{ext} is equal to the sum involving t_{ij}^{ext} in (30). Equation (38) shows how, in the case of homogeneous elasticity, the effect of elastic forces is equivalent to a certain two-point interaction.[170, 135] It is a singular interaction, however: it generally includes a delta-function at zero range, arising from the fact that the $\mathbf{k}$-space average of $\Psi_{ijmn}(\mathbf{k})$ is not zero. For anisotropic elasticity this interaction also decays very slowly at large distances, because its Fourier transform depends only on the direction of $\mathbf{k}$ and is therefore discontinuous as $\mathbf{k} \to 0$. In three dimensions,

$H_{ijmn}(\mathbf{x}-\mathbf{y})$ decays like the cube of the distance $|\mathbf{x}-\mathbf{y}|$, for distances small compared to the size of Ω.

In the special case where the material is isotropic (see Eq. (6)) as well as being elastically homogeneous and where the stress-free strain is a pure dilatation as in Eq. (4), only the delta-function component of H_{ijmn} is present, and Eq. (38) simplifies to

$$W=\frac{18KG}{3K+4G}\int_{\Omega}(q(\mathbf{x})-\bar{q})^2\,\mathrm{d}^3\mathbf{x}+W^{ext} \tag{39}$$

where $q(\mathbf{x})$ is defined to be q inside the inclusions and 0 outside, and $\bar{q}$ is the space average of $q(\mathbf{x})$. The result (39), without the term W^{ext}, is due to Cahn (1961).[222] He writes the expression in front of the integral sign more neatly as $2E/(1-\nu)$, where E is Young's modulus and ν is Poisson's ratio.[11]

The question of what formula replaces (38) if the elastic stiffness matrix is heterogeneous (i.e., different in the two phases) was considered by Onuki in 1989[135] for isotropic elasticity and in 1990[117, 116] for a cubic crystal. Treating the inhomogeneity as a small perturbation, he found that to first order of perturbation the elastic energy could be expressed as the sum of three parts

1. a long-range interaction due to the anisotropy;
2. a dipolar interaction which is proportional to the external stress and to the amount of inhomogeneity;
3. a non-quadratic "Eshelby" interaction proportional to the amount of inhomogeneity.

Khachaturyan *et al.* (1995)[50] carried this type of analysis further, considering higher orders of perturbation. They found that in the lowest order of perturbation the inhomogeneity is equivalent to a four-point interaction; in the next order, to a six-point interaction, and so on.

2.1.4. Two Theorems

Theorem 1 (Eshelby (1956)[231, 223]). If the elasticity tensor λ_{ijmn}, the external stress tensor t_{ij}^{ext}, and the stress-free strains e_{ij}^{α} and e_{ij}^{β} in the two phases are independent of position, then W^{ext} depends only on the total volume of the inclusions and not on their sizes, shapes, number or arrangement.

[11] Young's modulus and Poisson's ratio are related to the shear and bulk moduli by $K=E/3(1-2\nu)$, $G=E/2(1+\nu)$. See, for example, Gurtin.[200]

Proof. By the conditions of the theorem, the tensor e_{ij}^{ext} defined just after Eq. (33) is independent of position. Hence Eq. (10) can be written

$$\begin{aligned} W^{ext} &= -\sum_{ij} e_{ij}^{ext} \int_{\Omega} \sum_{mn} \lambda_{ijmn} e_{mn} \, \mathrm{d}^3\mathbf{x} \\ &= -\sum_{ij} e_{ij}^{ext} \int_{\Omega} \left(t_{ij} + \sum_{mn} \lambda_{ijmn} e_{mn}^0 \right) \mathrm{d}^3\mathbf{x} \qquad \text{by (13)} \\ &= -\sum_{ij} e_{ij}^{ext} \left\{ \int_{\Omega} t_{ij}^{ext} \, \mathrm{d}^3\mathbf{x} + \sum_{mn} \lambda_{ijmn} (|\Omega^\alpha| \, e_{mn}^\alpha + |\Omega^\beta| \, e_{mn}^\beta) \right\} \end{aligned} \tag{40}$$

by (21). This last expression depends on the inclusions only through their total volume. ▌

Theorem 2 (The "Bitter-Crum" theorem).[12] Under the conditions of Theorem 1, if in addition the elasticity tensor and the stress-free strain tensor are isotropic, then for an infinite or periodic specimen the elastic energy W depends only on the total volume of the inclusions, not on their sizes, shapes, positions etc.

Proof. For periodic boundary conditions, the result follows from the formula (39), since the integral is equal to $|\Omega^\alpha| \, (q^\alpha - \bar{q})^2 + |\Omega^\beta| \, (q^\beta - \bar{q})^2$ and is therefore independent of how the inclusions are arranged. For an infinite system, the integral in (39) is replaced by one over all space, and since $\bar{q}$ is now equal to q^β, the integral is equal to $|\Omega^\alpha| \, (q^\alpha - q^\beta)^2$ and is again independent of how the inclusions are arranged. ▌

Both theorems, especially the first, are somewhat counter-intuitive. The first theorem tells us that in order to explain rafting using linear elasticity theory we must either use a heterogeneous stiffness tensor or else have more than one type of inclusion so that the stress-free strain can be different in different inclusions. (For further information about general theorems relating to rafting, see ref. 37.) The second theorem tells us, as John Cahn has always seen very clearly,[45] that if there is to be an elastic interaction affecting the shape or separation of inclusions then at least one of the following conditions must be violated:

1. Matrix and inclusion(s) have the same elastic stiffness tensor,

[12] It was first pointed out by Bitter[236] that in in a linearly elastically istropic material there is no elastic interaction between two inclusions of a certain type, and Crum[235] (also, independently, Robinson[234]) showed how to generalize this result to a wider class of inclusions. See also Eshelby 1957, 1959.[229, 227] The name "Bitter-Crum" theorem was, apparently, devised by John Cahn.[162]

2. The strain characterizing the misfit is isotropic (i.e., purely dilatational),
3. The elasticity tensor is isotropic,
4. The crystal has no boundaries (i.e., it is infinite, or periodic),
5. The stress depends linearly on the displacement field.

As we shall see, different violations produce different effects on the coarsening behaviour.

2.2. Energy Calculations for Isotropic Elasticity

In the rest of this chapter we consider some applications of the static sharp interface model. In the present section we shall use the approximation that both the stiffness tensor and the stress-free strain are isotropic. Although real metals are always anisotropic, such calculations are useful because they can be used to investigate the effect of elastic heterogeneity (i.e., of violations of condition 1 of the Bitter-Crum theorem). Effects due to anisotropy will be considered in the following Section 2.3.

2.2.1. Elementary Calculations with Isotropic Elasticity and Misfit. We consider first two types of inclusion whose elastic energies in an infinite matrix can be calculated quite easily, the plate (slab) and the sphere. To allow for the possibility of finite volume fractions, in which case it is not obvious *a priori* which phase will constitute the inclusions and which the matrix, we shall allow the stress-free strain to differ from zero in both phases, being given by the isotropic formula (4) but with different values for q in the two phases. The object of the calculations is to find the space-averaged energy per unit volume and also the space-averaged strain (which gives information about the response to an externally applied stress).

Plate-Shaped Inclusions. Consider a configuration consisting of alternating slabs of the two phases, the slabs of phase α having thickness h^α, those of phase β having thickness h^β. Denote the normal to the faces of the slabs by $\mathbf{n}$. The equations of elastic equilibrium have a solution in which the strain in the α phase has the form

$$e_{ij}^\alpha = Q^\alpha \delta_{ij} + P^\alpha(\delta_{ij} - 3n_i n_j) \tag{41}$$

where P^α and Q^α are constants, and similarly for the β phase. The total energy per unit volume of material can be calculated from Eq. (6); for an

isotropic stress-free strain, as given by Eq. (4) generalized to allow for non-zero values of q in each of the two phases, it is

$$\bar{w} = \{\tfrac{9}{2}K^\alpha(Q^\alpha - q^\alpha)^2 + 6G^\alpha(P^\alpha)^2\}\ \phi + \{\tfrac{9}{2}K^\beta(Q^\beta - q^\beta)^2 + 6G^\beta(P^\beta)^2\}(1-\phi) \tag{42}$$

where $\phi = h^\alpha/(h^\alpha + h^\beta)$ is the volume fraction of phase α.

The expression (42) is to be minimized subject to the coherence constraint (15), which because of (3) and (41) is now

$$P^\alpha + Q^\alpha = P^\beta + Q^\beta \tag{43}$$

(This minimization automatically takes care of the stress continuity condition (16)). The minimum value, which gives the actual mean energy density of this system of inclusions, is

$$\bar{w} = \frac{9\phi(1-\phi)}{2} K_*[q]^2 \tag{44}$$

where K_* is defined by

$$\frac{1}{K_*} = \frac{1-\phi}{K^\alpha} + \frac{\phi}{K^\beta} + \frac{3}{4}\left\{\frac{1-\phi}{G^\alpha} + \frac{\phi}{G^\beta}\right\} \tag{45}$$

In the limit where the volume fraction of the precipitates goes to zero, (this includes the case of a single plate-like inclusion in an infinite matrix) the energy per unit volume *of precipitate* is

$$\lim_{\phi \to 0} \bar{w}/\phi = \frac{18K^\alpha G^\alpha [q]^2}{3K^\alpha + 4G^\alpha} \tag{46}$$

If there is a small externally applied stress, the resulting energy can be found from the average strain at zero applied stress, using (10). The anisotropic (deviatoric) part of this average strain is

$$\bar{e}_{ij} - \frac{1}{3}\sum_k \bar{e}_{kk} = -(\phi P^\alpha + (1-\phi)\ P^\beta) = \frac{3}{4}\left(\frac{1}{G^\alpha} - \frac{1}{G^\beta}\right) K_*[q] \tag{47}$$

We shall not need the isotropic part.

It is not hard to generalize these results to a cubic crystal, if $\mathbf{n}$ is in a convenient direction. If $\mathbf{n}$ is along one of the crystal axes, it is only necessary to replace K by $(C_{11} + 2C_{12})/3$ and G by $(C_{11} - C_{12})/2$ in the various formulas. If $\mathbf{n}$ is along the $[111]$ direction, G should instead be replaced by C_{44}.

Spherical Inclusion. Consider a spherical inclusion of α phase, of radius R_1, embedded in a larger sphere of β phase having radius R_2. Putting the centres of both spheres at the origin, we look for a solution in the form

$$\mathbf{u} = \begin{cases} Q^\alpha \mathbf{x} & (|\mathbf{x}| < R_1) \\ Q^\beta \mathbf{x} + P\nabla \dfrac{1}{|\mathbf{x}|} & (R_1 < |\mathbf{x}| < R_2) \end{cases} \tag{48}$$

where Q^α, Q^β and P are scalar constants. Since $\mathbf{u}$ is radial in both solutions, the coherency condition (15) can be satisfied by making

$$Q^\alpha R_1 = Q^\beta R_1 - P/R_1^2 \tag{49}$$

Using (3) we find that the strain is

$$e_{ij} = \begin{cases} Q^\alpha \delta_{ij} & (|\mathbf{x}| < R_1) \\ Q^\beta \delta_{ij} + P(3x_i x_j - |\mathbf{x}|^2 \delta_{ij})/|\mathbf{x}|^5 & (R_1 < |\mathbf{x}| < R_2) \end{cases} \tag{50}$$

Hence, by (6), the elastic energy is

$$\begin{aligned} W &= \frac{4\pi R_1^3}{3} \frac{9K^\alpha}{2} (Q^\alpha - q^\alpha)^2 + \frac{4\pi(R_2^3 - R_1^3)}{3} \frac{9K^\beta}{2} (Q^\beta - q^\beta)^2 \\ &\quad + \int_{R_1}^{R_2} 6G^\beta \left(\frac{P^\beta}{r^3}\right)^2 4\pi r^2 \, \mathrm{d}r \\ &= \frac{4\pi R_2^3}{3} \left\{ \frac{9K^\alpha}{2} (Q^\alpha - q^\alpha)^2 \phi + \frac{9K^\beta}{2} (Q^\beta - q^\beta)^2 (1-\phi) \right. \\ &\quad \left. + 6G^\beta (Q^\beta - Q^\alpha)^2 \phi(1-\phi) \right\} \end{aligned} \tag{51}$$

where $\phi = (R_1/R_2)^3$ is the volume fraction of phase α, and we have used (49) to eliminate P in the second line.

The expression (51) is to be minimized with respect to Q^α and Q^β. The minimum value can be written in the form $(4\pi R_2^3/3)\,\bar{w}$, where $\bar{w}$, the actual space-averaged elastic energy per unit volume, is given by

$$\bar{w} = \frac{9\phi(1-\phi)}{2} K_\bullet [q]^2 \tag{52}$$

with $K_\bullet$ defined by

$$\frac{1}{K_\bullet} = \frac{1-\phi}{K^\alpha} + \frac{\phi}{K^\beta} + \frac{3}{4G^\beta} \tag{53}$$

In the limit of zero ϕ, which includes the case of a single spherical inclusion in an infinite matrix, the energy per unit volume of inclusion is

$$\lim_{\phi \to 0} \bar{w}/\phi = \frac{18K^{\alpha}G^{\beta}[q]^2}{3K^{\alpha} + 4G^{\beta}} \tag{54}$$

For this geometry, the space average of the strain is purely isotropic, and so (by (10)) the linear part of the energy of a spherical inclusion due to an externally applied field is zero.

Conclusions. From these elementary calculations we can draw some tentative conclusions about the effects of elastic inhomogeneity on the energetically preferred configurations of the precipitates, provided that elastic anisotropy does not mask these effects.

First of all, a comparison of Eqs. (54) and (46) shows that if $G^{\alpha} > G^{\beta}$, that is if the inclusion is more rigid than the matrix, then the sphere has lower energy than the plate; on the other hand if the inclusion is less rigid than the matrix, then the plate configuration has the lower energy. That is to say, a spherical inclusion is likely to be stable only if it is stronger (more rigid) than the surrounding matrix. If it is justified to use Eq. (52) to estimate the energy of a system of spherical inclusions even when ϕ is not vanishingly small then one can go even further: this formula, when compared with (44), suggests that a system of spherical inclusions made from the more rigid material will always have a lower energy than the alternating plate configuration with the same ϕ, so that in addition to destabilizing soft spherical inclusions elastic heterogeneity tends to destabilize all plate-like inclusions. (A similar argument, based on the energies of elliptical and ellipsoidal inclusions, is given in ref. 7.)

Secondly, Eq. (47) shows that for an alloy where the more rigid material also has a larger stress-free volume (the correlation between size and strength we all remember from the school playground) the space-averaged strain for plate-like inclusions is a contraction in the direction perpendicular to the plate and an expansion in the directions parallel to it. The formation of such an inclusion in the presence of an externally applied stress tending to make the inclusions thicker will require more energy than for an external stress tending to make them thinner (see Eq. (10)). Consequently, in such a material, a plate-like inclusion will tend to align perpendicular to an externally applied uniaxial compressive stress, but parallel to an externally applied uniaxial tensile stress. In symbols

$$\begin{aligned} &t^{ext}_{axial}[q][G] > 0 \Rightarrow \text{inclusions parallel to axis of applied stress} \\ &t^{ext}_{axial}[q][G] < 0 \Rightarrow \text{inclusions perpendicular to } \ldots \end{aligned} \tag{55}$$

where $t^{ext}_{axial} = (2t^{ext}_{33} - t^{ext}_{11} - t^{ext}_{22})/3$ is the axial component of the anisotropic part of the applied stress (taking this axis to be along the 3 axis), which is positive (negative) for a tensile (compressive) stress.[13]

These conclusions can be understood physically in the following way: in the case of a spherical inclusion, the matrix is sheared but the inclusion is not, so the sphere is a good (low-energy) configuration when the matrix is very flexible. On the other hand, for a plate-shaped inclusion, only the inclusion is sheared, and so when the inclusion is very flexible the plate is a better shape than a sphere. Moreover if, in addition to being softer than the matrix, the plate has a lower stress-free density, then the matrix will prevent it from contracting in the direction parallel to the plate; it can only contract in the direction perpendicular to the plate, and hence the anisotropic part of the strain is a contraction in this direction, and plate-like inclusions will be energetically favoured when the stress is tending to compress them.

2.2.2. The Energy of a Single Inclusion: Isotropic Elasticity. For most shapes of inclusion other than sphere, cylinder and plate the calculation of elastic fields is complicated, but Eshelby[229, 227, 223] showed how to do it for an ellipsoidal inclusion. He found that if the inclusion is more (less) rigid than the matrix, an ellipsoid has more (less) elastic energy than a sphere of the same volume. Thus, a spherical inclusion which is more rigid than the matrix is stable against deformation to an ellipsoid, but (disregarding the stabilizing effect of the surface energy) one that is is softer than the matrix is unstable. This result is consistent with the comparison in the previous section between a spherical inclusion and a plate, which can be regarded as an infinitely flat ellipsoid. The comparison remains essentially the same if the misfit strain is anisotropic.[34]

The mere fact that one can calculate the energy exactly for an ellipsoid does not, of course, prove that this is the equilibrium shape, since an energy calculation alone does not show that the equilibrium condition (27) is satisfied. Kaganova and Roitburd[156, 148, 139] showed that the ellipsoid really is the equilibrium shape (and the ellipse in two dimensions), even when the stress-free strain is anisotropic, and determined the ranges of parameter values for which it is stable. Later[127] they extended their analysis to the case where the inclusion (though not the matrix) is elastically anisotropic.

[13] The formulation (55) is given in ref. 36. According to Thompson and Voorhees,[26] this effect was predicted by Cahn soon after his 1961 work on spinodal decomposition: see ref. 216.

If we take surface energy into account as well as elastic energy, the energy per unit volume of inclusion depends on the size of the inclusion as well as its shape. This effect was first studied by Khachaturyan and his collaborators (1973, 1983),[197, 171, 170] for crystals with cubic symmetry. Their approximate calculations indicated that for inclusions smaller than a certain size (which depends on the material) the equilibrium shape has cubic symmetry, whereas for larger inclusions it is plate-like. Johnson and Cahn (1984)[166] showed that the same symmetry-breaking transition is a general phenomenon, present even for isotropic elasticity. For small inclusions the surface term F^{Γ} in the free energy formula (2) predominates, and the shape of the lowest-energy inclusion has the same symmetry as that which minimizes the surface free energy F^{Γ} for a fixed volume of the inclusion. In the case of an isotropic surface tension this would be a sphere, but for anisotropic surface tension it could also be a polyhedron facetted parallel to the crystal planes where the surface tension is minimum. As the size is increased the elastic energy becomes more important and there is a transition, which may be either continuous or discontinuous, to a new equilibrium shape of lower symmetry. If an external stress is present, this too can induce a shape transition (Berkenpas *et al.* (1986),[150] Johnson *et al.* (1988)[138]).

With a view to constructing a theory of rafting, Pineau (1976)[188] calculated the energies of single elliptical inclusions in an externally applied stress field, using methods devised by Eshelby.[223] A brief comparison of his predictions with experiment is given by Socrate and Parks (1993).[82]

2.2.3. The Energy of Two or More Inclusions: Isotropic Elasticity. In the absence of elastic forces, the mechanism of coarsening arises from the fact that a pair of spherical inclusions with given total volume have less total surface energy the more unequal their sizes. To see how this mechanism is influenced by elastic forces, we would like to know how the elastic energy of a pair of inclusions depends on their size and separation. Can they reduce their elastic energy by transferring material from one inclusion to another, or by changing their separation?

For isotropic elasticity, calculations of this type were first done by Eshelby in 1966.[214] For a pair of spherical inclusions with radii R_1, R_2 and centres a distance D apart, he found the energy of interaction to be approximately

$$W_{int} = \frac{8\pi}{81}\left(\frac{1+\nu}{1-\nu}\right)^2 [q]^2 [G] \left\{\frac{R_1^6 R_2^3}{(D^2-R_2^2)^3} + \frac{R_2^6 R_1^3}{(D^2-R_1^2)^3}\right\} + O([G])^2 \quad (56)$$

where $\nu = (3K-G)/(6K+2G)$ is Poisson's ratio and $[q]$, $[G]$ mean $q^{\alpha} - q^{\beta}$, $G^{\alpha} - G^{\beta}$, as before. If the inclusions are more rigid than the matrix,

then formula (56) says that the interaction energy is positive and (for fixed values of the separation D and the total volume $(4\pi/3)(R_1^3 + R_2^3)$) is least when the two inclusions are of equal size. This suggests that the elastic energy will tend to make the inclusions of equal size. This stabilizing effect, just the opposite of the tendency of surface energy to enlarge the large inclusions at the expense of the small ones, has been given the name "inverse coarsening."

In his papers drawing attention to the above stabilizing effect Johnson[169, 165] used a generalized version of the formula (56) which included also surface energy and the effect of an external stress. He concluded[169] that, in the absence of external stress, the inverse coarsening effect would occur whenever the size of the inclusions exceeded a certain threshold related to the critical size we have called R_0. He also found[165] that a uniaxial external tensile stress could favour or inhibit inverse coarsening depending on the angle between the separation of the inclusions and the axis of the external stress.

The elastic interaction of more complicated systems of inclusions of given shape has also been studied; for example Johnson and Voorhees (1987)[147] consider the elastic interaction energy of a system of several cuboids (rectangular prisms), finding a tendency of such precipitates to align, even though the medium is isotropic. Abinandanan and Johnson (1993)[75, 76] calculated the elastic interaction energy of two spherical inclusions with a tetragonal misfit strain. The energy is positive when the line joining the particles and the axis of the misfit are parallel, negative when they are perpendicular.

The value of all such conclusions based on the assumption of spherical precipitates is, however, called into question by the work of Onuki and Nishimori (1991).[105] They showed that the interaction energy is extremely sensitive to the shapes of the inclusions. Equation (56) assumes that the inclusions are spheres, but a small deformation of the spheres reduces the interaction to zero. Since there is no reason why the actual precipitates should be exact spheres, formula (56) cannot be relied on.

Two other calculations using pre-assigned shapes of inclusion are the energy calculations for a three-dimensional array of inclusions in the shape of square or rectangular plates by Perovic *et al.*[181] and the elastic stress calculations for two-dimensional arrays of square plates by Glatzel and Feller–Kriepmayer.[124]

2.3. Energy Calculations for Anisotropic Elasticity

In this section we use energy methods to investigate the effect of elastic anisotropy (usually with cubic symmetry) on coarsening—that is to say,

the effect of violating condition 3 rather than condition 1 of the Bitter-Crum theorem. Except where otherwise stated, the material is assumed to be elastically homogeneous.

2.3.1. The Energy of a Single Inclusion: Anisotropic Elasticity. Khachaturyan (1966)[215, 170] (see also Roitburd (1967),[212] Roitburd and Kosenko[189]) showed how to calculate the elastic energy of an arbitrary inclusion (or indeed an arbitrary system of inclusions), using the Fourier transform formula (31). This energy is minimized by making the inclusion a plate (or an array of parallel plates) with faces (the "habit planes") perpendicular to a vector $\mathbf{n}$ that minimizes the function $B(\mathbf{n})$ defined in (37). This configuration obviously satisfies the interfacial equilibrium condition (27) too. The directions of the minimizing vectors are called *elastically soft* directions. For a cubic crystal such as tungsten which has positive anisotropy, i.e., $C_{11} - C_{12} - 2C_{44} > 0$, the elastically soft (minimizing) directions are $[111]$, $[11\bar{1}]$ etc.; for negative anisotropy, as in Al, Cu, Fe, Ni, they are $[100]$, $[010]$ and $[001]$. Analogous calculations for non-isotropic inclusions are given in ref. 176.

The elastic energy of some other shapes of inclusion can also be found analytically, for example spheres, ellipsoids,[208, 209] and cubes.[185, 170] If the strain in the inclusion is uniform (i.e., for all these shapes except the cube), the energy can also be calculated for a material which is elastically heterogeneous as well as anisotropic[187] (see Section 8.4 of ref. 170).

When surface energy is taken into account, the minimum-energy shape of the inclusion is no longer a plate; moreover, as noted in our discussion of the isotropic case (Section 2.2.2), the minimum-energy shape depends on the size of the inclusion. The (effectively) two-dimensional calculations of Khachaturyan and Hairapetyan[197, 170] illustrate how the minimum-energy shape, round when the inclusion is very small, can pass through a succession of more and more needle-like shapes as the inclusion is made larger. For a crystal with square symmetry, as the size of the inclusion is increased there is a transition from minimum-energy shapes with fourfold (square) symmetry to ones with twofold symmetry.[73, 39] (Symmetry-breaking transitions of a similar kind occur for isotropic elasticity: see Section 2.2.2).

In three dimensions, the minimum-energy shape is more difficult to compute; a common procedure has been simply to compare the energies of various easily calculable shapes such as spheres, ellipsoids, cubes, cuboids, tetrahedra and octahedra and to assume that the actual shape at a given volume of inclusion will be similar to the easily calculated shape having the least energy. Such calculations[141, 128, 124, 91] show that the precipitate may pass thorough a variety of different minimum-energy shapes as its size is increased, and may even split into two or more smaller pieces. As we have

mentioned in Section 1.2.1, splitting of this kind has been observed experimentally with γ' precipitates in nickel-base and other superalloys:[174, 158, 128, 71] see Fig. 4. A review of all such energy calculations up to 1992 is given by Johnson and Voorhees.[88, 87]

The effect of an externally applied stress on the energy-minimizing shape of an ellipsoidal inclusion with elastic forces only, a key factor in the theory of rafting, was studied by Chang and Allen (1991),[99] following earlier theoretical work by Tien and Copley (1971),[202] Pineau (1976)[188] (mentioned in Section 2.2.2 above), Miyazaki *et al.* (1979),[180] Johnson (1987)[146] (who showed that the true equilibrium shape could be approximated by an ellipsoid of revolution), and Johnson *et al.* (1988)).[138] Using realistic elastic constants, Chang and Allen find good agreement with observed shapes and orientations. Their article also contains a good critical review of the earlier theoretical work on rafting. Nabarro *et al.* (1996)[36] consider a cubic crystal with inclusions having the shape of tetragonal prisms instead of ellipsoids, and they find that Eq. (55) holds, with the shear modulus G replaced by its analogue for a cubic crystal, which is (see the paragraph after (47)) $(C_{11} - C_{22})/2$ if [100] is a soft direction.

The restriction of working within a pre-selected set of shapes (spheres, cuboids, etc.) is avoided in the work of McCormack *et al.* 1992[90] who do an unusual type of two-dimensional finite-element computation in which, as the size of the inclusion is increased, its shape follows a path of steepest descent with respect to energy, not even requiring the topology to stay the same. As the size of the inclusion is increased, the round shape first turns into a square, and later on a nucleus appears inside the square (or on the surface if the calculation forbids changes of topology) and the square splits into two or four. More recently Schmidt and Gross[56, 25] using a boundary integral method to solve the equilibrium equation (27) for a cubic crystal, studied the dependence of the shape of the inclusion not only on its size but also on the misfit strain (assumed purely dilataional) and various elasticity parameters. The most important of these turned out to be the ratio of the rigidities of the inclusion and the matrix. When the inclusion is less rigid than the matrix, its faces (if it is large enough) can be partly concave; also it can become unstable against elongation.

2.3.2. The Energy of Several Inclusions: Anisotropic Elasticity. As in the case of isotropic elasticity, we study pairs of inclusions in order to understand when inverse coarsening can take place, and if it does what relative position of the inclusions gives the least energy. In addition, there is the possibility we have already mentioned (see Fig. 4) that a single inclusion may be able to reduce its energy by splitting into two (or more) parts.

Several authors have,studied these questions by investigating the energy of a pair of spherical inclusions. Johnson and Lee (1979)[179] show that two spherical inclusions in an anisotropic matrix can reduce their energy if they come close together and align themselves along the "soft" crystal directions. Miyazaki, Doi and others[154, 86, 80] find in addition that inverse coarsening is possible if the particles are close together and the misfit strain and particle size are large enough. Shneck *et al.* (1992)[93] give details of the elastic fields for one and two spherical inclusions in a cubic crystal with negative anisotropy.

Inclusions shaped like cubes and cuboids have also been studied, because of their relevance to the observed splitting of such inclusions in γ' precipitates. Doi *et al.* (1984)[163] showed that a single cuboid may have more elastic energy per unit volume of precipitate than an array of eight cuboids, or a pair of parallel plates. Khachaturyan *et al.* (1988)[141] compare the energy of a cube-shaped inclusion, in a cubic crystal having negative anisotropy, with that of two half-cubes and with an octet of smaller cubes. Depending on the distances involved, either the doublet or the octet can have lower energy than the single cube.

The most up-to-date calculations are those of Schmidt *et al.*[15] who calculate the true minimizing configuration and take into account the possibility of elastic heterogeneity. Contrary to the homogeneous case, the elastically heterogeneous two-inclusion system can have an energy minimum, implying the possibility of inverse coarsening.

2.3.3. Positional Correlations. We have already noted that a pair of inclusions of given shape often has the least energy if the inclusions are close together and are aligned along an elastically soft direction. The same tendency was found in arrays consisting of a large number of inclusions, by Khachaturyan and his collaborators.[207, 170, 195] They found, for example, that in a cubic alloy with negative anisotropy the minimum-energy array for a system of spherical inclusions is a simple cubic superlattice.

3. THE DYNAMIC SHARP-INTERFACE MODEL

3.1. Modelling Diffusion

The dynamic version of the sharp-interface model differs from the static version in taking account of the mechanism of time evolution, which is diffusion. Since diffusion arises from concentration gradients, we drop the assumption made in the static version of the sharp-interface model that the intrinsic properties of the alloy are uniform in each phase. The composition

of the alloy will now depend on position; but the elastic stiffness matrix and the stress-free strain tensor will still be assumed uniform within each phase, though in general different in different phases.

For simplicity, let us assume that the alloy consists of just two types of atom, A and B, so that the local composition of the alloy can be described by a single field, the local concentration of A atoms, which we denote by c. We shall assume that the concentration of A atoms in the β phase is small so that c is small in the β phase. In the α phase, we assume that c is close to its zero-temperature equilibrium value in that phase which we denote by c_0^α. If the α phase is pure A, then $c_0^\alpha = 1$, but it is also possible for c_0^α to be less than 1; for example in an Ni-Al alloy the precipitates have a Ni_3-Al structure so that for this alloy the equilibrium concentration of Al atoms in the precipitates is $c_0^\alpha = 1/4$.

3.1.1. The Diffusion Equation and Its Boundary Conditions. Within each phase, the concentration varies with time by diffusion, which we can model by the standard diffusion equation[14]

$$\frac{\partial c}{\partial t} = \nabla \cdot (D \nabla c) \tag{57}$$

For simplicity, we shall take the diffusivity D to be uniform in each phase, though it may take different values in different phases.

The motion of the interface is controlled by the net rate of arrival of A atoms, in accordance with the standard mass conservation formula associated with (57),

$$v_n[c] = -[D\mathbf{n} \cdot \nabla c] \tag{58}$$

where $\mathbf{n}$ is a unit vector normal to Γ and v_n denotes the velocity of Γ (with respect to the undistorted lattice) in the direction of $\mathbf{n}$.

To use these equations we need two conditions to determine the values of c on the two sides of Γ. Since these conditions are also satisfied at equilibrium, we can obtain approximations to them by formulating the two conditions that must be satisfied on Γ at equilibrium. One of these conditions refers to the possibility of mass transfer across Γ, the other to the possibility of motion of Γ relative to the underlying lattice.

The condition for equilibrium under mass transfer across Γ is that the chemical potentials of the two kinds of atoms on the two sides should be equal. Denoting the chemical potential of A relative to B (i.e., the excess of

[14] If the elasticity tensor and/or stress-free strain depend on concentration, a more complicated equation is necessary; see Eq. (86) below.

the chemical potential of A over that of B) by μ, we can write this condition

$$\mu^{\alpha} = \mu^{\beta} \qquad \text{on } \Gamma \tag{59}$$

where μ^{α} (or μ^{β}) denotes the limiting value of μ at any point on Γ as that point is approached from within the α (or β) phase.

If the system is not in equilibrium, extra terms may appear in (59) depending, for example, on the velocity of the interface (corresponding to the kinetic undercooling term in the theory of freezing and melting). We shall assume here, however, that the deviation from equilibrium is small enough to justify neglecting such terms.

In defining the chemical potentials which appear in (59), we must take account of the elastic contribution to the free energy, defining it as the derivative of the total free energy with respect to particle number at constant strain. However, since we are taking the stiffness matrix and the stress-free strain to be independent of concentration in each phase, it follows from the formula (5) for the strain energy that the elastic contribution to the free energy does not affect the chemical potential. The formula giving the chemical potential (of A relative to B) is therefore just the same as it would be in the absence of elastic energy:

$$\mu(c) = \frac{df(c)}{dc} \tag{60}$$

(If temperature variations were of any importance, we would of course write $(\partial f/\partial c)_T$, but ln a metal it is reasonable to treat all processes as isothermal.)

To obtain our second condition, we consider the condition for equilibrium under displacements of the interface. This can be obtained by requiring the total free energy to be a minimum with respect to variations of Γ subject to the constraint that the number of A particles, denoted here by N^A, is fixed:

$$N^A = \int_{\Omega} c \, \mathrm{d}^3\mathbf{x} = \text{const.} \tag{61}$$

The argument closely follows the corresponding one in Section 2.1.2, with the constant-volume constraint used there (see Eq. (22)) replaced by (61), and the resulting necessary condition for a minimum, analogous to (27), is

$$2\sigma\kappa + [\, f + w \,] - \sum_{ik} T_i [\, u_{i,k} \,] \, n_k = \mu [\, c \,] \tag{62}$$

where $[c] = c^\alpha - c^\beta$ is the discontinuity in c across the interface. We have denoted the Lagrange multiplier by μ in accordance with the general princple that the Lagrange multiplier is equal to the derivative of the minimum value with respect to the value of the constraint, which in this case is dF/dN^A, i.e., the chemical potential μ. At equilibrium, μ, μ^α and μ^β are all the same, and as in the case of Eq. (59) we shall make the approximation of neglecting any non-equilibrium terms in (62), proportional to, say, the velocity of Γ, even when the system is not in equilibrium.

The condition (62) (without the curvature term) appears to be due to Robin[196] and, in greater generality, to Larché and Cahn (1978).[184] The elastic terms in this equation are part of what Eshelby[206, 190] calls the "energy-momentum tensor." The curvature term, which incorporates the Gibbs–Thomson effect, was included by Cahn and Larché (1982),[172] following earlier work by Gurtin and Murdoch (1975)[191] on surface stresses in solids.

3.1.2. The Generalized Gibbs–Thomson Condition. Equation (62) can be brought to a more convenient form, generalizing the Gibbs–Thomson formula. For each phase we introduce (following Larché and Cahn (1973)[198]) a thermodynamic potential π, the grand canonical pressure, referring to the properties of this phase at zero stress. Considered as a function of c, it is defined by

$$\pi(c) = c\mu(c) - f(c) \tag{63}$$

so that

$$\frac{d\pi(c)}{dc} = c\frac{d\mu}{dc} \tag{64}$$

The interface condition (62) can now be written

$$[\pi] = 2\sigma\kappa + [w] - \sum_{ik} T_i [u_{i,k}]\, n_k \tag{65}$$

where $[\pi]$ means $\pi^\alpha - \pi^\beta$, that is $\pi(c^\alpha) - \pi(c^\beta)$.

To obtain convenient approximate formulas for μ and π, consider first their values at the type of equilibrium normally considered in thermodynamics, for which the interfacial curvature is small and the lattices in the two phases are incoherent, so that surface and elastic energies play no part in the equilibrium conditions. At such an equilibrium Eq. (59) shows that there will be a common value of μ^α and μ^β; denote this common value by μ_{eq}. Moreover, Eq. (65) reduces in this case to $[\pi] = 0$; that is to say, π^α and π^β have a common value at such an equilibrium. Denote this

common value by π_{eq}, and the values of c in the two phases at such an equilibrium by c^{α}_{eq} and c^{β}_{eq}.

By Taylor's expansion about this point of incoherent equilibrium (and, in the second line, the use of (64)), we have the following approximations which are useful in the α phase:

$$\mu(c^{\alpha}) = \mu_{eq} + \mu'(c^{\alpha}_{eq})(c^{\alpha} - c^{\alpha}_{eq}) + O(c^{\alpha} - c^{\alpha}_{eq})^2 \tag{66}$$

$$\pi(c^{\alpha}) = \pi_{eq} + c^{\alpha}_{eq}\mu'(c^{\alpha}_{eq})(c^{\alpha} - c^{\alpha}_{eq}) + O(c^{\alpha} - c^{\alpha}_{eq})^2 \tag{67}$$

where the prime denotes a derivative with respect to c. There is a similar approximation for the β phase. It follows from (66) and (67) that

$$\pi(c^{\alpha}) = \pi_{eq} + c^{\alpha}_{eq}(\mu(c^{\alpha}) - \mu_{eq}) + O(\mu(c^{\alpha}) - \mu_{eq})^2 \tag{68}$$

From this we can subtract the corresponding formula for $\pi(c^{\beta})$, and using also the condition (59) in the form $\mu(c^{\alpha}) = \mu(c^{\beta})$, we obtain

$$[\pi] = [c_{eq}](\mu - \mu_{eq}) + O(\mu - \mu_{eq})^2 \tag{69}$$

where μ denotes the common value of $\mu(c^{\alpha})$ and $\mu(c^{\beta})$. Re-arranging (66), and then using (69), we get the approximate formula

$$c^{\alpha} - c^{\alpha}_{eq} = \frac{\mu - \mu_{eq}}{\mu'(c^{\alpha}_{eq})} = \frac{[\pi]}{[c_{eq}]\,\mu'(c^{\alpha}_{eq})} \tag{70}$$

in which $[\pi]$ is to be evalueated from (65).The formula for $c^{\beta} - c^{\beta}_{eq}$ is analogous.

For the model alloy we are considering here, the chemical potential can be expanded in virial-type expansions about the two points c^{α}_0 and c^{β}_0. If we take c^{β}_0 to be zero for simplicity, and in a case such as Ni_3Al neglect the small concentration of minority atoms on the sites preferred by majority atoms, these expansions have the form

$$\begin{aligned} \exp\frac{\mu(c) - \mu_{eq}}{\mathrm{k}T} &= \frac{c}{c^{\beta}_{eq}}\,\{1 + O(c)\} \\ \exp\frac{\mu_{eq} - \mu(c)}{\mathrm{k}T} &= \frac{c^{\alpha}_0 - c}{c^{\alpha}_0 - c^{\alpha}_{eq}}\,\{1 + O(c^{\alpha}_0 - c)\} \end{aligned} \tag{71}$$

where k is Boltzmann's constant and T is the temperature. The reason why $\mu(c)$ appears with a negative sign in the second equation is that in the α phase the small parameter of the virial expansion is $c^{\alpha}_0 - c$, the concentration

of B atoms, and the relative chemical potential of these atoms is $-\mu(c)$. Using (71) in (70), we obtain the approximate formulas

$$c^{\alpha} = c^{\alpha}_{eq} + \frac{(c^{\alpha}_0 - c^{\alpha}_{eq})[\pi]}{kT[c_{eq}]}, \qquad c^{\beta} = c^{\beta}_{eq} + \frac{c^{\beta}_{eq}[\pi]}{kT[c_{eq}]} \tag{72}$$

in which $[\pi]$ stands for the expression on the right side of (65). An example showing how the differential equation and boundary conditions formulated in this section are used is given in the following section.

The formula (72), reducing in the absence of elastic effects to the Gibbs–Thomson formula, is due to Leo and Sekerka[130] (see also refs. 144, 75, 39). Earlier, Johnson and Alexander[152] had obtained a similar equation and used it to calculate c at the surface of a spherical inclusion with isotropic elasticity.

3.2. Sharp-Interface Evolution Calculations

3.2.1. Growth or Shrinkage of an Isolated Spherical Inclusion. In this section we calculate (following Laraia *et al.*[142, 129]) the rate of growth of a spherical inclusion of radius R in an infinite elastically isotropic matrix, with the boundary condition that c approaches a prescribed limit c^{∞} far from the inclusion. At the surface of the inclusion its value is given by (72). The calculations are simple because the geometry makes $[\pi]$, and therefore c^{α} and c^{β}, independent of position on Γ.

We make the approximation (which appears to be a good one if $R\,dR/dt \ll D$) of neglecting the time derivative in the diffusion equation (57), so that it reduces to Laplace's equation. The appropriate solution, with origin at the centre of the sphere, is

$$c = \begin{cases} c^{\alpha} & (r < R) \\ c^{\infty} + (c^{\beta} - c^{\infty})\, R/r & (r > R) \end{cases} \tag{73}$$

where r means $|\mathbf{x}|$. Using (58) we find the rate of growth of the inclusion to be

$$\frac{dR}{dt} = v_n = \frac{D}{[c]}\left[\frac{dc}{dr}\right]_{r=R} = -\frac{D(c^{\beta} - c^{\infty})}{[c]\,R} \approx -\frac{D(c^{\beta} - c^{\infty})}{[c_{eq}]\,R} \tag{74}$$

If there are no elastic forces, then (65) reduces to $[\pi] = 2\sigma/R$, and so, using (72) to evaluate c^{β}, we obtain

$$\frac{dR}{dt} \approx \frac{2\sigma D c^{\beta}_{eq}}{kT[c_{eq}]^2\,R}\left(\frac{1}{R^*} - \frac{1}{R}\right) \tag{75}$$

where R^*, defined by $(c^\infty - c^\beta_{eq}) = 2\sigma c^\beta_{eq}/\mathrm{k}T[c_{eq}]\,R^*$, is the so-called critical radius, the radius of an inclusion at whose surface the value of c^β would be c^∞.

If elastic forces are present, then Eq. (65) can be evaluated using the $R_2 \to \infty$ limit of the solution for a spherical inclusion outlined in Section 2.2.1. The result is

$$[\pi] = 2\sigma/R + 18K^\alpha G^\beta [q]^2/(3K^\alpha + 4G^\beta) \tag{76}$$

Equation (75) still holds, with R^* now defined by

$$2\sigma/R^* = \mathrm{k}T[c_{eq}](c^\infty - c^\beta_{eq})/c^\beta_{eq} - 18K^\alpha G^\beta [q]^2/(3K^\alpha + 4G^\beta) \tag{77}$$

Equation (75) is a central component of the LSW theory of coarsening at very low volume fractions of precipitate, which we have already mentioned in Section 1.2.2 and shall discuss further in Section 3.2.4. In that theory each precipitate has its own value of R, which changes with time according to Eq. (75). The common value of R^* is determined by requiring the total volume of the precipitates to be conserved. LSW argue that both R^* and the average radius of the precipitates will grow in proportion to $t^{1/3}$. Since Eq. (75) is unaffected by the presence of the elastic term in (76) it follows[129] that the elastic term has no effect whatever on the coarsening behaviour as predicted by the LSW theory. The elastic effects will be revealed only by going beyond the main assumptions made in the above calculation, which are that the elasticity is isotropic, the precipitates are spherical, and their volume fraction is very small.

3.2.2. A Single Nonspherical Inclusion. We have already seen in Section 2.2.2 that a spherical inclusion, with isotropic elasticity, can be thermodynamically unstable if it is softer than the matrix. If the inclusion is growing, a further instability becomes possible, corresponding to the one discovered by Mullins and Sekerka[219] for the non-elastic case; it appears as soon as a certain critical radius (which depends on the rate of growth) is exceeded. This type of instability has been investigated using linear theory by several authors.[118, 131, 106, 78]

The first application of the sharp-interface model to nonlinear time evolution of the shape of a precipitate was a two-dimensional calculation by Voorhees, McFadden and Johnson (1992),[95] using a boundary integral method to solve the diffusion equation in the matrix (they neglected diffusion inside the precipitates). They calculated the shape evolution of a single precipitate of arbitrary initial shape for an anisotropic system having the elastic constants of Ni-Al, choosing the concentration at infinity so that the volume of the precipitate remained constant as it approached

an equilibrium shape. In contrast to the energy calculations described in Section 2.3.1, they did not find any symmetry-breaking transitions: the equilibrium shape always had fourfold symmetry even if the initial shape did not, and their precipitates never split into pieces; they attribute this to their not having considered such large precipitates (i.e., such large values of R/R_0) as the other workers.

Jou *et al.* (1997)[18] did similar calculations, but they used isotropic elasticity and chose the concentration at infinity so that the precipitate would grow at a prescribed rate. The mass influx has a big effect on the shape, favouring the formation of dendrites both for relatively hard and relatively soft precipitates, whereas the equilibrium shapes are "squarish." If there is an external stress field, the dendrites perpendicular and parallel to the axis of this field grow at different rates.

3.2.3. Two or Three Precipitates. When studying more than one precipitate, or even a single precipitate in three dimensions, it is a complicated task to follow the detailed evolution of the boundary surfaces. To avoid the difficulty, some authors constrain the precipitates to be spherical, determining the rate of change of the size and position of each sphere from appropriate integrals of Eq. (58) over the surface of that sphere. Voorhees and Johnson (1988),[145] also Johnson *et al.* (1989),[126] studied two spherical precipitates in an isotropic matrix, solving the diffusion equation in the matrix using bispherical coordinates. For precipitates that are softer than the matrix, they find inverse coarsening if the ratio of the particle radii is less than about 2. Diffusion also makes the centres of the precipitates move; they move in the non-elastic case too, but here the movement is faster. Johnson *et al.* (1990)[114] extend this type of calculation to anisotropic elasticity. They find inverse coarsening when the precipitate separation is along a soft direction, but coarsening rates are enhanced for some other directions of the separation.

Getting away from the assumption of spherical precipitates, Su and Voorhees (1996)[39, 40] did 2-D calculations for a pair (or triplet) of inclusions in a matrix with cubic symmetry, allowing for shape changes (but not for diffusion inside the precipitates). Large precipitates adopted approximately rectangular shapes, rather than the round ones assumed in fixed-shape calculations. Inverse coarsening was never observed for two-precipitate systems (notwithstanding the results of earlier calculations at fixed shape); in systems of three precipitates, local inverse coarsening was observed but it was never enough to stabilize the system as a whole against further coarsening. With regard to the movement of the precipitates, the main effect of the elastic forces was to align pairs of precipitates so that the line joining their centres was along one of the elastically soft directions. These

forces also caused the precipitates to move close together (partly by motion of their centres, partly by shape changes), but not to touch. In discussing these results the authors make use of the concept of configurational forces due to Eshelby[233] and Gurtin.[3]

3.2.4. Many Precipitates: The LSW Theory. The first theory of coarsening, which took no account of elastic interactions, was the LSW theory, which we have already outlined in Section 3.2.1. This theory, which assumes that the volume fraction of precipitates is vanishingly small, predicts that the average radius of the precipitates present at time t will grow in proportion to $t^{1/3}$; and, as we have seen, this conclusion is unaffected by the elastic energy (assumed isotropic).

For finite volume fractions the simple LSW theory becomes inaccurate because the precipitates are no longer independent. The predictions of the theory can be improved upon by following numerically the individual sizes of a sample system of precipitates which are assumed to be spherical (for reviews, see Voorhees[161, 96]). Enomoto and Kawasaki (1988,1989)[140, 122] carried out numerical simulations of this type in which the effect of isotropic elasticity was included by means of Eshelby's formula (56) for the elastic interaction between two spherical inclusions. The diffusion potential at the surface of an inclusion was replaced by an average value over that surface, calculated in terms of the partial derivative of the total free energy with respect to the radius of the inclusion. For precipitates that were harder (i.e., more rigid) than the matrix, they found that the elastic interaction assisted the coarsening mechanism and indeed speeded it up so that the average radius eventually grew in proportion to $t^{1/2}$ instead of $t^{1/3}$; at the same time, the distribution of particle sizes became broader than that predicted by LSW. On the other hand, if the precipitates were softer than the matrix, the elastic interaction was found to slow down the coarsening or even stop it altogether, and the distribution of particle sizes became much narrower than that of LSW (another manifestation of inverse coarsening).

A serious disadvantage of the simulations of Enomoto and Kawasaki is that they depend on Eshelby's formula (56) for the elastic interaction, which in turn depends on an assumpton that the precipitates are spherical. As pointed out by Onuki and Nishimori (1991)[105] (see Section 2.2.3 above) if the precipitates are allowed to change their shape, the interaction energy may deviate greatly from this formula and so these simulations do not even convincingly establish the $t^{1/2}$ growth law.

Shortly after these simulations were done Leo *et al.*[115] gave a general scaling argument leading to the conclusion that when the precipitates are large enough for the surface tension to be unimportant the average linear

size of the precipitates will indeed grow in proportion to $t^{1/2}$. Their argument is based on the same idea as one given by Mullins and Viñals[155, 133] which predicts a $t^{1/3}$ growth law for the case where there are no elastic forces. The main assumption used in this argument is that the domain structure is statistically self-similar, i.e., that at any time it has the same statistical properties as the one obtained by a uniform expansion of the domain structure at any earlier time. However, in contrast to the capillarity-dominated case, where there is plenty of evidence for the statistical self-similarity hypothesis and the $t^{1/3}$ law is well-established, in the case where elastic forces dominate there appear to be many cases, particularly for anisotropic materials, where the hypothesis of self-similarity is false. For example, the hypothesis would require the equilibrium shape of a single inclusion to be independent of its size, but for anisotropic elasticity this is not so (see Section 2.3.1 above). The scaling argument does, however, tend to confirm the $t^{1/2}$ growth law found by Enomoto and Kawasaki for spherical precipitates which were harder than the matrix.

Another feature of coarsening that has received much attention in the nonelastic case is the positional correlations. For the elastic case, the first study of positional correlations using the sharp-interface method was done by Abinandanan and Johnson (1993). They calculated[75, 76] the concentration field in a three-dimensional isotropic matrix containing spherical inclusions, using a multipole expansion method. (For an alternative to the multipole expansion method, see ref. 66). Unlike Enomoto and Kawasaki, they took the elastic stiffness matrix to be homogeneous, but they avoided the Bitter-Crum theorem by making the misfit strain tetragonal rather than isotropic. They obtained the effect of diffusion in the matrix (though not inside the precipitates) not only on the sizes of the precipitates but also on their velocities. The resulting formulas were used in a simulation of the time evolution of a system of spherical precipitates whose initial positions and sizes were chosen from a random distribution. In the final configuration, the positions of most of the surviving precipitates were strongly correlated: arranged in a plane perpendicular to the axis of the tetragonal misfit strain if the axial component of the anisotropic part of the misfit strain was an expansion, but in lines parallel to the misfit strain axis if this component of the misfit strain was a compression. In a later paper[43] Abinandanan and Johnson discuss the development of spatial correlations during coarsening. For small particles, capillary forces dominate and the particles hardly move; the spatial correlation is that each relatively large particle is surrounded by a depletion zone from which it has eaten most of the solute material. For large particles, elastic forces dominate and the particles do move, setting up a new system of correlations characterized by clustering of favourably oriented similarly sized particles.

Hort and Johnson (1996)[32] simulate the time evolution of a system of spherical precipitates in the presence of a uniaxial applied stress, both for homogeneous elasticity with tetragonal misfit strain and for heterogeneous elasticity with isotropic misfit strain. The precipitates are found to align themselves in a way that is consistent with Eq. (55).

All the calculations mentioned so far in this section depend on the (dangerous) simplifying assumption of spherical precipitates. Jou *et al.* (1997)[18] do two-dimensional calculations which do take shape changes into account, using the boundary integral method mentioned in Section 3.2.2. Their calculations refer to an elastically isotropic but heterogeneous material. Complicated effects are observed: alignment, movement, coagulation, coarsening, with everything depending strongly on the amount of elastic inhomogeneity, the misfit strain, and the externally applied field.

4. DIFFUSE INTERFACE MODELS

In this type of model we no longer represent the phase boundary as a geometrical surface. Instead, the micro-structure of the interface is itself included in the model. The concentration $c(\mathbf{x}, t)$ of the A-component is now treated as a function of position $\mathbf{x}$ and time t which is continuous throughout the whole of Ω. The surface Γ and the domains Ω^α and Ω^β play no part in the mathematical formulation of these models, though it may be possible to identify them approximately once the concentration field is known. In particular, at late stages of the coarsening process, large domains develop in which c is almost uniform, being close to one or other of the equilibrium values c^α_{eq} and c^β_{eq} defined in Section 4.2; these domains, which are the analogues in this model of the domains Ω^α and Ω^β used in the sharp-interface model, are separated by a relatively thin transition layer whose thickness does not change with time, and which is the analogue of the geometrical surface Γ in the sharp-interface model.

An advantage of the method is that it gives information about the very early stages of spinodal decomposition, before any well-defined interfaces have formed.[222] For the late stages, it has further advantages: no a priori assumption about the topology of the interface need be made—this topology is determined by the evolution of the model itself—and in numerical work the difficult problem of dealing with moving free boundaries is avoided. Moreover, even when the topology does not change, the rather complicated conditions on the surface of Γ need not be allowed for explicitly.

4.1. The Cahn–Hilliard Equation and Some of Its Relations

4.1.1. The Cahn–Hilliard Equation. The diffuse-interface method was introduced in Cahn's celebrated paper about spinodal decomposition (1961).[222] He based his initial discussion on a formula, due originally to van der Waals,[237] for the free energy of a non-uniform system without elastic energy

$$F = \int_{\Omega} [f(c) + \tfrac{1}{2}\chi(\nabla c)^2]\, d^3\mathbf{x} \tag{78}$$

Here c (meaning $c(\mathbf{x}, t)$) is the concentration field, assumed to be a continous (indeed differentiable) function of position; $f(c)$ is the free energy density of the material at concentration c; and χ is a positive constant, so that the gradient term penalizes rapid spatial variations of c. For the approximations underlying this model to work, the length scale of these spatial variations should be large compared with the interatomic distance. In particular, the value of $c(\mathbf{x})$ at a given point $\mathbf{x}$ hardly depends on whether the atom nearest the point $\mathbf{x}$ is of type A or type B; rather, it represents the concentration of solute particles averaged over a region centred at $\mathbf{x}$ which is large enough to contain many particles.

To include phase transitions in the model, the function f is assumed to have a non-convex graph, as illustrated in Fig. 6. For example the approximation to f given by the mean-field theory of a binary substitutional alloy,

$$f(c) = \mu_{eq} c + 2kT_0 c(1-c) + kT\{c \log c + (1-c)\log(1-c)\} \tag{79}$$

where μ_{eq} and T_0 are constants, has a non-convex graph when $T < T_0$.

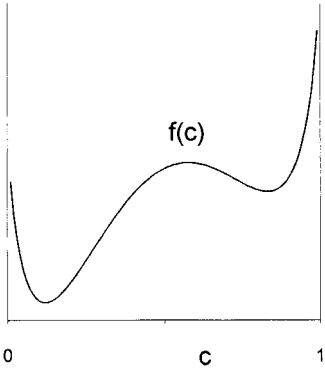

Fig. 6. A typical free-energy density function f.

For the time dependence of c, Cahn assumed

$$\frac{\partial c}{\partial t} = \nabla \cdot \left(M \nabla \frac{\delta F}{\delta c(\mathbf{x})} \right) \tag{80}$$

where M is a mobility coefficient, which may depend on c, and $\delta F/\delta c(\mathbf{x})$ is the variational derivative of F with respect to $c(\mathbf{x})$. The variational derivative is defined by the condition that

$$\int_{\Omega} \frac{\delta F}{\delta c(\mathbf{x})} \phi(\mathbf{x}) \, d^3\mathbf{x} = \left(\frac{dF(c + \varepsilon\phi)}{d\varepsilon} \right)_{\varepsilon = 0} \tag{81}$$

for all differentiable functions ϕ which vanish on the boundary of Ω. With F given by (78) this definition gives

$$\frac{\delta F}{\delta c(\mathbf{x})} = f'(c(\mathbf{x})) - \chi \nabla^2 c(\mathbf{x}) \tag{82}$$

where $f'(c)$ denotes the derivative of $f(c)$, the same thing as the local chemical potential used in Section 3.1, and so (80) becomes

$$\frac{\partial c}{\partial t} = \nabla \cdot M \nabla (f'(c(\mathbf{x})) - \chi \nabla^2 c(\mathbf{x})) \tag{83}$$

This is the Cahn–Hilliard equation, which is the cornerstone of the theory of spinodal decomposition without elastic interactions. If the formula (79) is used for f, M is generally taken to be $Dc(1-c)/\mathrm{k}T$ where D is the diffusivity (assumed for simplicity to be independent of c—compare Eq. (57)), so as to make (83) reduce to Fick's law when $c(1-c)\, T_0/T$ and χ are small.

Equation (83) is to be solved with boundary conditions modelling the conditions at the surface of the material, and initial conditions modelling the initial concentration distribution. For example, to represent an alloy quenched from a high temperature to a point inside the miscibility gap of the phase diagram, $c(\mathbf{x}, 0)$ is generally taken (see, for example, ref. 119) to be $\bar{c} + \zeta(\mathbf{x})$, where $\bar{c} = N^A/|\Omega|$ is the space-averaged concentration of A atoms and ζ is a spatially random function representing small concentration fluctuations. If the uniform state $c(\mathbf{x}) = \bar{c}$ is unstable (see Section 4.2 below) these fluctuations grow with time, eventually producing concentration distributions very similar to the ones that are observed experimentally in spinodal decomposition if elastic interactions are unimportant.

For many alloys, further order parameters besides the concentration are necessary to characterize the phase transition completely. The prototype of

such situations is the order-disorder transition at constant concentration, as in Cu-Au, where at low temperatures each kind of atom prefers one of two sublattices of a body-centred cubic lattice. The mathematical model uses an order parameter field $\eta(\mathbf{x})$ which is the local concentration of (say) Cu atoms on one of the sublattices. The free-energy functional has the form (78) with η replacing c, but since η does not obey a conservation law the kinetic equation is not (80) but the Allen–Cahn[178] equation

$$\frac{\partial \eta}{\partial t} = -\Lambda \frac{\delta F}{\delta \eta(\mathbf{x})} \tag{84}$$

(also known as the time-dependent Ginzburg-Landau equation) where Λ is a kinetic coefficient, which may depend on η. In general, both the concentration field and one or more order parameter fields will appear in the free-energy functional, the concentration obeying an equation of the form (83) and each non-conserved order parameter obeying an equation of the form (84).[15]

A further refinement of these equations, which makes it possible to allow for fluctuation effects such as nucleation, is to include noise terms on the right sides of (83) and (84). This development was initiated by Cook.[204] The resulting equations might be called the stochastic Cahn–Hilliard and stochastic Allen–Cahn equations. For further information about their use in physics see the reviews by Gunton *et al.*[167] or Gunton and Droz.[168] On the mathematical side, it is known that the stochastic Allen–Cahn equation with space-time white noise has a solution (indeed a unique solution) in one dimension, but in more than one dimension it appears that a solution exists only for coloured noise (with power spectrum falling off sufficiently rapidly at large wave numbers). The stochastic Cahn–Hilliard equation, on the other hand, appears to have a solution for white noise in up to three dimensions.[157, 5]

4.1.2. Including Elastic Energy in the Cahn–Hilliard Equation. The free energy formula (78) can be generalized to include elastic interactions if we introduce a new field variable $\mathbf{u}(\mathbf{x})$ and replace f by $f + w$ just as we did in (2). In order for the elastic interaction to have any effect, however, we must allow λ_{ijmn} and/or e^0_{ij} to depend on c, so that the elastic

[15] In principle, cross-terms might appear in these equations, for example, if there are two order parameters, $\partial \eta_1/\partial t = -\Lambda_{11}(\delta F/\delta \eta_1) - \Lambda_{12}(\delta F/\delta \eta_2)$.

energy density w now depends on c as well as the strain. The free energy formula thus becomes

$$F\{c(\cdot), \mathbf{u}(\cdot)\} = \int_{\Omega} [f(c(\mathbf{x})) + w(c(\mathbf{x}), e_{11}(\mathbf{x}),...) + \tfrac{1}{2}\chi(\nabla c(\mathbf{x}))^2]\, d^3\mathbf{x} \quad (85)$$

with $w(c, e_{11}, e_{12},..., e_{33})$ given by the formula (5), as before. The c-dependence of w arises from the possibility that λ_{ijmn} and e^0_{ij} may depend on c.

The functions f and w in (85) are defined in just the same way as for the sharp-interface model (see Eq. (2)); that is, $f(c)$ is the free energy density of the bulk material when the concentration is c and the (macroscopic) elastic stress is zero, and w is defined so that $f + w$ is the total free energy density of the bulk material. We shall continue to call w the elastic energy, but it might better be called the macroscopic elastic energy, since part of the c-dependence of $f(c)$ arises from microscopic elastic effects which are not visible on the macroscopic scale. Thus, if the A and B atoms are of different sizes, then when some of the atoms in an initally pure B lattice are replaced by A atoms the B lattice will be locally distorted, increasing its energy quite apart from any chemical interactions between the two kinds of atom. This type of microscopic interaction was first studied by Eshelby[231] and its role in the microscopic theory of solid solutions was developed by Khachaturyan.[211, 170]

Cahn's recipe (80) now gives, in place of (83), the generalized diffusion equation

$$\begin{aligned}\frac{\partial c}{\partial t} &= \nabla \cdot M \nabla \left(f'(c(\mathbf{x})) + \frac{\partial w(c(\mathbf{x}), e_{11}(\mathbf{x}),...)}{\partial c} - \chi \nabla^2 c(\mathbf{x}) \right) \\ &= \nabla \cdot M \nabla (\hat{\mu} - \chi \nabla^2 c(\mathbf{x})) \end{aligned} \quad (86)$$

where $\hat{\mu}$ is the *diffusion potential*, a function of c and $e_{11}, e_{12},...$ defined by

$$\begin{aligned}\hat{\mu} &= \frac{\partial (f(c) + w(c, e_{11}, e_{12},...))}{\partial c} \\ &= \mu(c) + \frac{1}{2} \sum_{ijmn} \frac{d\lambda_{ijmn}}{dc} (\Delta e)_{ij} (\Delta e)_{mn} - \sum_{ijmn} \lambda_{ijmn} (\Delta e)_{ij} \frac{de^0_{mn}}{dc} \end{aligned} \quad (87)$$

according to the formula (5) for w. Equation (86), without the gradient term, is due to Larché and Cahn.[173] The complete equation was given by Onuki (1989).[134]

In using Eq. (86) the elastic field variable $\mathbf{u}$ is assumed to relax to its equilibrium value much faster than the concentration, and therefore it is determined, just as in the sharp-interface model, by minimizing F. The

Euler–Lagrange equation for the minimization is, as in the sharp interface model, Eq. (11). In consequence of this minimization, the strain at each point in the material is a (non-local) functional of the entire density profile $c(\cdot)$ and so the diffusion potential at that point is likewise such a functional. For an example, see Eq. (91) below.

As in the sharp interface model, the minimization to find $\mathbf{u}$ is easiest for periodic boundary conditions, with the elastic stiffness tensor taken to be independent of c and therefore uniform so that the Fourier transform formula (38) can be used. A convenient way to allow for the dependence of stress-free strain on concentration in this formula is to assume a linear relation analogous to Vegard's law:

$$e^0_{ij} = a_{ij} + b_{ij} c \tag{88}$$

where a_{ij} and b_{ij} are consants which can be expressed in terms of the quantities e^α_{ij}, c^α_{eq} etc. used in Chapter 3. By substituting this into Eq. (38) and using the result in (85) we can express the free energy as a functional of the field c alone:

$$F\{c(\cdot)\} = \int_\Omega \{f(c(\mathbf{x})) + \tfrac{1}{2}\chi(\nabla c(\mathbf{x}))^2\}\, \mathrm{d}^3\mathbf{x} + \tfrac{1}{2} \iint_\Omega (c(\mathbf{x}) - \bar{c})\, V_{el}(\mathbf{x}-\mathbf{y})(c(\mathbf{y}) - \bar{c})\, \mathrm{d}^3\mathbf{x}\, \mathrm{d}^3\mathbf{y} \tag{89}$$

where $\bar{c}$ is the space average of c, and V_{el} is defined by

$$V_{el}(\mathbf{z}) = \sum_{ijmn} b_{ij} H_{ijmn}(\mathbf{z})\, b_{mn} \tag{90}$$

(a function whose spatial average is zero). Apart from a numerical factor $[c_{eq}]^{-2}$, V_{el} is the inverse Fourier transform of the function B in Khachaturyan's formula (36). When F is given by (89) the diffusion potential at $\mathbf{x}$ is the functional derivative of the non-gradient part of F with respect to $c(\mathbf{x})$, i.e.,

$$\hat{\mu}(\mathbf{x}) = \mu(c(\mathbf{x})) + \int_\Omega V_{el}(\mathbf{x}-\mathbf{y})(c(\mathbf{y}) - \bar{c})\, \mathrm{d}^3\mathbf{y} \tag{91}$$

where $\mu(c) = f'(c)$ is the chemical potential as in (60). The non-local character of the diffusion potential is evident from (91).

To obtain information about coarsening from such models, one must integrate (86) over long time intervals. Methods of integrating the non-elastic version of this equation are reviewed in ref. 121. The elastic calculation is

a formidable one, particularly in three dimensions, since to find $\partial w/\partial c$ the equation of elastic equilibrium (11) must be solved at each time step—either as a partial differential equation in position space, or (if the elastic constants are independent of concentration) by the Fourier transform formula (31) or an equivalent position-space formula such as the convolution integral in (91). Until recently it was not possible to calculate time evolution from these equations with any accuracy in a reasonable time, and inaccurate or uncertain methods had to be used instead;[143, 123] but more reliable methods are now becoming available.[2, 8]

In the limit where $\chi \to 0$, with a suitable concurrent re-scaling of the time variable, the Cahn–Hilliard equation (83) converges to the non-elastic version of the dynamic sharp-interface equations, formulated in Chapter 3.1. This was shown formally by Pego[136] and rigorously by Alikakos *et al.*[63] The corresponding convergence problem for the elastic version, Eq. (86), is treated by Leo *et al.* (1998).[8]

4.1.3. Lattice Differential Equations. The Cahn–Hilliard equation does not take explicit account of the lattice structure of the crystal. In the case where the elastic stiffness tensor is uniform, it is possible to take account of this lattice structure, without departing from the general philosophy of the method, if we replace the integral in (89) by a sum over N lattice sites $\mathbf{p}$ situated at positions $\mathbf{x}_\mathbf{p}$ in the periodic box Ω, so that the free energy functional F is approximated by a function of the N variables $c_\mathbf{p} = c(\mathbf{x}_\mathbf{p})$:

$$F = \frac{|\Omega|}{N} \sum_{\mathbf{p}} f(c_\mathbf{p}) + \frac{|\Omega|^2}{2N^2} \sum_{\mathbf{p}} \sum_{\mathbf{p}'} V(\mathbf{p}-\mathbf{p}')(c_\mathbf{p} - \bar{c})(c_{\mathbf{p}'} - \bar{c}) \tag{92}$$

Here V is defined by

$$V(\mathbf{p}) = \Delta(\mathbf{p}) + V_{el}(\mathbf{x}_\mathbf{p}) \tag{93}$$

with $\Delta(\mathbf{p})$ chosen so that $\sum_\mathbf{p} \sum_{\mathbf{p}'} \Delta(\mathbf{p}-\mathbf{p}')\, c_\mathbf{p} c_{\mathbf{p}'}$ is a finite-difference approximation to $\chi(\nabla c(\mathbf{x}_\mathbf{p}))^2$. For example, on a simple cubic lattice with lattice spacing a, we could take $\Delta(\mathbf{p}) = \chi/a^2$ for the 6 lattice points nearest to $\mathbf{p} = \mathbf{0}$, $\Delta(\mathbf{0}) = -6\chi/a^2$, and $\Delta(\mathbf{p}) = 0$ for all other lattice points. However, once the free energy has been written in the discrete form (92), new possibilities become available, since the non-elastic forces can now be allowed for explicitly instead of through their contribution to the thermodynamic free energy density $f(c)$. For example, $V(\mathbf{p})$ could be chosen to be negative (favouring unlike pairs of atoms) if the vector $\mathbf{p}$ connects a nearest-neighbour pair of sites but positive (favouring like pairs) if $\mathbf{p}$ connects a next-nearest neighbour pair. Free-energy formulas of this type are the basis of Khachaturyan's discussion[221, 217, 218] of equilibrium structures in crystals.

The discrete version of the Cahn–Hilliard kinetic equation (80) is

$$\frac{dc_{\mathbf{p}}}{dt} = \sum_{\mathbf{r}'} M_{\mathbf{p},\mathbf{p}'} \left(\frac{\partial F}{\partial c_{\mathbf{p}'}} - \frac{\partial F}{\partial c_{\mathbf{p}}} \right) \tag{94}$$

where F is given by (92) and the non-vanishing entries in the "mobility matrix" $M_{\mathbf{p},\mathbf{p}'}$ take a value proportional to the mobility M used in (80). Equation (94) is due to Khachaturyan[211, 170] and, independently, Hillert, Cook *et al.*[224, 203] It was introduced into this field by Chen and Khachaturyan.[100, 101]

A difficulty with most derivations of (94), including the one just given, is that although we know how to define M when c is the same at all lattice sites—a suitable formula is $M(c) = \text{const.}\, Dc(1-c)/\mathrm{k}T$ as in the continuous-space formula given just after Eq. (83)—it is not obvious how to define $M_{\mathbf{p},\mathbf{p}'}$ when $c_{\mathbf{p}}$ and $c_{\mathbf{p}'}$ are different. Microscopic derivations leading to equations of this type[192, 108] give (provided $c_{\mathbf{p}}$ does not vary too rapidly from one site to the next) a formula corresponding approximately to (94) with $M_{\mathbf{p},\mathbf{p}'}$ replaced by $M(\frac{1}{2}(c_{\mathbf{p}} + c_{\mathbf{p}'}))$ or $\frac{1}{2}M(c_{\mathbf{p}}) + \frac{1}{2}M(c_{\mathbf{p}'})$. Another possiblity is the proposal of Koyama and Miyazaki (1998)[51, 6] to treat the right side of (94) as a constant times a finite-difference approximation to $\nabla \cdot \{ M(c(\mathbf{x}_{\mathbf{p}}))\, \nabla \mu(\hat{\mathbf{x}}_{\mathbf{p}}) \}$ so that it can be replaced by the same constant times a finite-difference approximation to the equivalent expression $M(c(\mathbf{x}_{\mathbf{p}}))\, \nabla^2 \mu(\hat{\mathbf{x}}_{\mathbf{p}}) + \nabla M(c(\mathbf{x})) \cdot \nabla(\partial F/\partial c(\mathbf{r}))$. However in most computations $M_{\mathbf{p},\mathbf{p}'}$ has simply been given the constant value $M(\bar{c})$, regardless of the local value of c. For the results of computations based on (94) see Section 4.3 below.

4.2. The Stability of a Uniform Mixture

4.2.1. Isotropic Elasticity. It was pointed out by Cahn (1961),[222] that the elastic energy term w in the free energy expression (2) tends to stabilize a homogeneous mixture which in its absence (that is to say, if the requirement of elastic coherence were removed) might be expected to separate into two phases. In his original paper he showed that this effect exists even in an isotropic solid.[16]

[16] The "Bitter-Crum" theorem might seem to imply that istropic homogeneous elasticity never has any effect, and indeed if the microscopic interactions are modelled by treating the solute atoms as spheres in an istropic elastic medium (Eshelby's model[231, 170]) then for a coherent lattice the total elastic energy is independent of $c(\mathbf{x})$ at fixed $\bar{c}$, since $f(c)$ contains a term $\eta^2 Ec(1-c)/(1-\nu)$ whose contribution to the integral in (96) just cancels the effect of the macroscopic elasticity term $\eta^2 E(c-\bar{c})^2/(1-\nu)$. Cahn's idea, however, is to compare the coherent lattice with an incoherent lattice having the same function f but no macroscopic elasticity term. For further discussion, see refs. 170 and 47. Equation (96) itself is perfectly consistent with the Bitter-Crum theorem, which indeed can be derived from it by omitting the gradient term and then giving $c(\mathbf{x})$ different constant values in the two phases.

The mixture is assumed to obey Vegard's law, that the stress-free strain is isotropic and varies linearly with the concentration, so that

$$e_{ij}^0 = \eta(c - c_0)\,\delta_{ij} \tag{95}$$

where η and c_0 are constants. Then we can insert the formula (39) for the macroscopic elastic energy into (85) and obtain, in the absence of externally applied strain,

$$F = \int_\Omega \left(f(c(\mathbf{x})) + \frac{\eta^2 E}{1-\nu}(c(\mathbf{x}) - \bar{c})^2 + \frac{1}{2}\chi(\nabla c)^2 \right) \mathrm{d}^3\mathbf{x} \tag{96}$$

where $\bar{c} = \Omega^{-1}\int_\Omega c(\mathbf{x})\,\mathrm{d}^3\mathbf{x}$. The uniform state with $c(\mathbf{x}) = \bar{c}$ everywhere is stable if F is a minimum with respect to variations of c satisfying the constraint $\int (c - \bar{c})\,\mathrm{d}^3\mathbf{x} = 0$. It is stable against all such variations if and only if the function $f(c) + (\eta^2 E/(1-\nu))(c - \bar{c})^2$ is convex, and it is stable against small variations if and only if this function is locally convex near $c = \bar{c}$, that is to say if

$$f''(\bar{c}) + 2\eta^2 E/(1-\nu) > 0 \tag{97}$$

where f'' denotes the second derivative of the function f. The elastic term can make the left-hand side of (97) positive even though $f''(\bar{c})$ is negative, and so the coherent mixture can be stable against phase separation even though an incoherent mixture of the same composition would not be. This effect can lower the critical temperature of such mixtures significantly. For a discussion of this and related effects using a simple thermodynamic model see Cahn and Larché (1984).[162]

4.2.2. Anisotropic Elasticity. The above treatment of stability is easily generalized to anisotropic elasticity (Cahn (1962)[220]). Substituting Vegard's law (95) into (31) we obtain, in the absence of externally applied stress,

$$\begin{aligned} W &= \frac{1}{2|\Omega|}\sum_{\mathbf{k}\neq 0}\sum_{im}\eta^2\,|c(\mathbf{k})|^2\,\Psi_{iimm}(\mathbf{k}) \\ &\geqslant \frac{\eta^2}{2|\Omega|}\sum_{\mathbf{k}\neq 0}|c(\mathbf{k})|^2 \min_{\mathbf{k}}\sum_{im}\Psi_{iimm}(\mathbf{k}) \\ &= \frac{1}{2}\eta^2 \min_{\mathbf{k}}\sum_{im}\Psi_{iimm}(\mathbf{k})\int_\Omega (c(\mathbf{x}) - \bar{c})^2\,\mathrm{d}^3\mathbf{x} \qquad \text{by Parseval's theorem} \end{aligned} \tag{98}$$

As in the discussion of (96), it follows that the uniform state is stable against small concentration fluctuations if

$$f''(\bar{c}) + \tfrac{1}{2}\eta^2 \min_{\mathbf{k}} \sum_{im} \Psi_{iimm}(\mathbf{k}) > 0 \tag{99}$$

This equation, in the form appropriate to a cubic crystal, is due to Cahn.[220] The elastic term is always positive (see the text just after Eq. (33) above) and therefore the macroscopic elastic interactions make the coherent mixture more stable against phase separation than the incoherent, just as they do for isotropic elasticity.[17]

A generalization of this kind of stability analysis, with the elastic moduli depending on concentration, has been used by Thompson and Voorhees[26] to discuss the effect of an externally applied stress on orientation of the newly-formed precipitates in an anisotropic alloy.

4.3. Simulations with the Diffuse Interface Model

4.3.1. A Single Precipitate. Wang *et al.*[110] carried out calculations for a single precipitate in a two-dimensional crystal with square symmetry and negative isotropy, using Khachaturyan's kinetic equation (94). The initial configuration was chosen to represent a single circular precipitate, and they waited for an equilibrium to be reached, for various different values of a parameter representing the ratio of the elastic to the short-range interactions in their model. Allowing for the difference between two and three dimensions, this parameter is proportional to the one denoted by $1/R_0$ in Section 1.1 of the present paper. As the parameter was increased (which corresponds to considering larger and larger precipitates in a real physical system) the equilibrium shape, at first round, became more and more square; then, a hole appeared in the middle of the square and finally it split into two rectangles. It is also possible for the faces of the "square" to become concave.[60] On the other hand, the transition to a single inclusion of only twofold symmetry, which is predicted by the

[17] Khachaturyan, in Chapter 13 of ref. 170, argues that (96) and its anisotropic generalization should be replaced by a different formula in which our $f(c)$ is replaced by $f(c)$ plus a term due to the microscopic elastic interactions. The difference of opinion appears to us to arise from different definitions of the symbol f; the physical conclusion that the coherent system is more stable than the incoherent one is the same whichever formula is used—see for example diagram 11 on p. 499 of ref. 170, according to which there are temperatures at which the incoherent system separates into two phases while the coherent system does not.

sharp-interface model (see Section 2.3.1), does not appear to have been observed with the diffuse-interface model. The reason for this is unclear.

In three dimensions there are even more possibilities, particularly if the transformation strain is anisotropic (Wang *et al.* (1996)[42]). However, as these authors show in ref. 62 the behaviour of isolated precipitates is not necessarily a reliable guide to their behaviour in the presence of others.

4.3.2. Many Precipitates. Nishimori and Onuki (1990)[116] carried out two-dimensional simulations using the elastic Cahn–Hilliard equation (86) with an anisotropic stiffness tensor. Starting from an initial concentration distribution corresponding to a homogeneous disordered state (i.e., a constant plus a small spatially random term), they found that the shapes of the precipitates were strongly affected by the elastic anisotropy, and that they tended to align themselves along the crystal axes. See Fig. 7d,e.

Wang *et al.*[111, 97, 85] (see also ref. 29), also did simulations on this type of system, but they used the Khachaturyan equation (94) and paid more attention to the effect of volume fraction and to to the visible details of the evolution process. For small volume fractions, the latest observed state consisted mostly of nearly round precipitates near the sites of a square superlattice. This configuration was reached by a form of inverse coarsening, in which the precipitates that were close to sites of the nascent superlattice grew at the expense of those that were not, regardless of the initial sizes of these precipitates. For larger volume fractions (say 50%) the precipitates, initially disconnected, tended to coalesce, and the latest observed state consisted of needle-like precipitates parallel to the two soft directions. In a later paper[61] these authors consider a case where the transformation strain is tetragonal rather than isotropic (modelling Mg-stabilized cubic ZrO_2); here the precipitates line up initially along crystallographic directions, but later an alternating band structure develops as the precipitates in some rows grow at the expense of those in others. Another tetragonal system, TiO_2-SnO_2, was studied by Nambu and Sato,[81] who found that a lamellar structure developed.

Koyama and Miyazaki[94, 6] used the Khachaturyan equation to simulate an Al-Zn alloy; they found coarsening but no positional ordering; on the other hand for Fe-Mo, where the mismatch is more than three times as big and the elastic moduli more than twice as big, they did find ordering. Another system studied by the same group is beta Ti-Cr, for which the method predicted (in agreement with experiment) extremely fine platelike precipitates distributed homogenously through the bcc matrix.[12]

Onuki and Nishimori (1991, 1992)[107, 92] were the first to investigate the effects of elastic inhomogeneity by means of this type of simulation. To isolate the effect of the inhomogeneity (which, confusingly, they call "elastic misfit" in some of their papers) they assumed isotropic elasticity. If the softer (less rigid) phase occupied less than half of the total volume, then at early times the configuration consisted of isolated precipitates of softer phase embedded in a matrix of the harder phase, but as coarsening proceeded these precipitates joined up to make a percolated network structure, so that it was now the harder phase which was arranged in isolated inclusions, while the softer phase formed the surrounding matrix (see Fig. 7(a–c)). Moreover, the growth of these precipitates was anomalously slow, i.e., slower than the usual $t^{1/3}$ law. Later, these authors did simulations of the same type for anisotropic (but still inhomogeneous) elasticity.[104] The anisotropy made the inclusions align themselves parallel to one of the crystal axes, but still the softer phase wrapped the harder one. If an external stress in an oblique direction was applied, the preferred directions of the inclusions tilted so as to be more nearly perpendicular to one of the principal axes of the external stress.

The numerical method used by Onuki and Nishimori for the time evolution was not an accurate one; later work using accurate methods (Leo

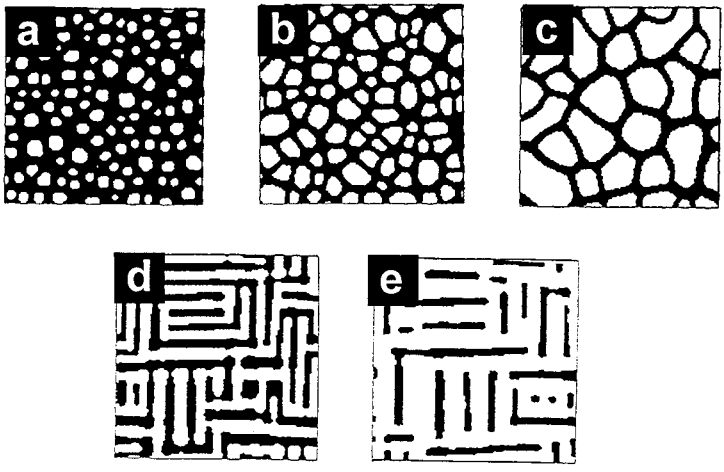

Fig. 7. Typical snapshot pictures for isotropic but heterogeneous elasticity (a–c) and homogeneous elasticity with cubic anisotropy (d–e) using equations of the type (85–86). In (a–c), the stiffer phase is shown white with volume fractions of 0.3, 0.5 and 0.7, respectively (from ref. 107). Note that the softer phase always wraps stiffer particles. In (d–e), the volume fraction of the white phase is 0.5 and 0.7, respectively (from ref. 116).

et al. 1998[8]) has, however, confirmed their conclusions about the reversal of the topological roles of the two phases.

These topological changes, which the sharp-interface model had failed to predict because it is not suited to following such changes, can nevertheless be understood qualitatively on the basis of the sharp-interface formula for spherical inclusions given in Section 2.2.1. According to that formula the energy per unit volume of precipitate is less for rigid precipitates in a flexible matrix than for flexible precipitates in a rigid matrix. Or, even more qualitatively, consider the extreme case where both phases have the same bulk modulus but one of the phases is perfectly flexible. i.e., its shear modulus is zero. If the inclusions are perfectly flexible the rigidity of the surrounding matrix will prevent them from taking up the sizes where their density has its stress-free value and therefore they will have some strain energy; but if the matrix is perfectly flexible then the (rigid) inclusions can take up their stress-free sizes and shapes and the matrix can expand or contract to its stress-free density, so that there is no strain energy at all. Thus the energy is lower for a perfectly flexible matrix than it is for perfecty flexible inclusions.

4.3.3. Ordered Phases. In alloys such as Ni-Al one of the phases (in this case the Ni_3-Al phase) can have more than one variant. Such systems can be treated using Khachaturyan's kinetic equation (94), generalized by incorporating additional order parameters as described at the end of Section 4.1.1. Simulations of various types of alloy requiring this type of treatment have been done by Sagui *et al.* (1994),[72] by Wang and Khachaturyan (1995),[62] by Li and Chen (1998)[10, 11] and by Wang *et al.* (1998).[16]

An important new possibility is that the transformation strain can be anisotropic and hence different in the different variants; then, when an external stress is applied, one variant will grow at the expense of another. In this way, since the conditions of Eshelby's theorem (see Section 2.1.4) do not apply, rafting can take place even with homogeneous elasticity. A recent paper by Le Bouar *et al.*[1] models the time evolution of alloys of this type in which the matrix is a cubic crystal but the precipitates are tetragonal, using a generalized stochastic Cahn–Hilliard equation with three dependent variables: the concentration and two order parameters. The theoretical model is spectacularly successful: see Fig. 2.

4.3.4. Thin Films. In this section we look at the possibility of elastic interactions arising from a violation of condition 4 of the Bitter-Crum theorem, that is to say in a system with boundaries. An effect of this type was noted by Larché and Cahn[89] who pointed out that if spinodal

decomposition takes place in an isotropic film with uniform elastic constants the equilibrium state can have the two phases on opposite faces of the film, and because of the elastic misfit the film will bend. This effect has indeed been observed, in the $\alpha - \alpha'$ phase separation of Nb-H.[182, 177] In these experiments, the hydrogen-rich α' phase was found on the outer side of simply curved specimen foils. In some cases the foil was even observed to split into two pieces with half thickness. Both halves were strongly curved. These results were interpreted as a spinodal decomposition process where the specimen thickness was equal to the spinodal wavelength for the simply curved foil and for each of the halves of the split foil.

Putting an appropriate approximation for the elastic strain field into the elastic Cahn–Hilliard equation (86) Larché and Cahn obtained the kinetic equation

$$\frac{\partial c}{\partial t} = \nabla^2 \left[\frac{df(c)}{dc} + \frac{2\eta^2 E}{1-\nu} \left(c - \bar{c} - \frac{3x}{2h} M_1^c \right) - \chi \nabla^2 c \right] \tag{100}$$

where η is the compositional expansion coefficient, defined in (95), E and ν are Young's modulus and Poisson's ratio, $\bar{c}$ is the average concentration, and M_1^c is the first moment of the concentration distribution in the direction at right angles to the film, defined by

$$M_1^c = \frac{1}{h^2} \int_{-h}^{h} (c - \bar{c})\, x \, \mathrm{d}x \tag{101}$$

Here h is half the thickness of the film and the coordinate system in the material is chosen to make the two faces of the unstrained film the planes $x = h$ and $x = -h$. The one-dimensional version of these equations, obtained by neglecting the dependence of c on y and z, was studied both analytically and numerically by Larché and Cahn, and numerically in more detail by Cahn and Kobayashi.[45] The most striking result was that the elastic term accelerated the separation into two phases.

Another bounded-system problem to which the diffuse-interface model can be applied is the growth of thin films by deposition, an important process in the semiconductor industry. The elastic problem is more complicated than before because there is now a misfit between the film and the substrate as well as the one due to compositional nonuniformity. Moreover, the possibility of surface diffusion[230, 137] and the effect of material arriving at the surface have to be allowed for. At the time of writing the implications of linear stability theory are still being worked out,[109, 83, 49, 31, 4, 9] though nonlinear effects are clearly important too.[84]

5. ATOMIC LATTICE MODELS

5.1. The Born Model

In this approach continuum elastic theory is abandoned; instead the elastic properties of the material are obtained by considering the mechanical forces between individual atoms. Each atom is assiged a definite site **p** on the lattice, whose position when the lattice is undistorted we denote (as in Section 4.1.3) by $\mathbf{x_p}$, and the displacements $\mathbf{u_p}$ of the atoms from these sites are assumed to be small enough to justify using the harmonic approximation, i.e., treating the force on each atom as a linear function of all the atomic displacements of all the atoms. The way to calculate the macroscopic elastic properties of a crystal from the interatomic force parameters is explained in the book by Born and Huang (1954),[232] and, by doing the calculation in reverse, the interatomic force parameters can be obtained from phonon dispersion curves. For simplicity, we assume that only two-body forces act, so that atoms which are close enough together to interact can be thought of as being joined by springs. However, one should not be misled by this picture into assuming that all the atomic interactions are necessarily central forces; this assumption would imply certain relations.between the elastic constants (sometimes called Cauchy relations)[232] which are violated in many real materials. For example in a crystal with cubic symmetry the Cauchy relation is $C_{12} = C_{44}$ which, although a good approximation for some ionic crystals, is a very bad one in most metals.

In the case of an alloy, the interaction between two atoms depends not only on their separation but also on their nature. It is usual to think of their interaction energy as the sum of two parts, one of which, the so-called chemical interaction, depends only on what kind of atom they are and not on their positions; the other part, the elastic interaction, does depend on their positions and has a minimum value of zero which is achieved for some relative position. This energy-minimizing relative position depends on the nature of the two atoms: one can think of the two kinds of atoms as being of different sizes, and the natural length of the spring joining the centres of two atoms as being the sum of the radii of the atoms. The stiffness of the spring may also depend on the nature of the two atoms. The theory of the equilibrium properties of solid solutions based on this type of model has been developed by Khachaturyan[211, 170] and by Cook and de Fontaine (1969, 1971, 1972).[205, 201, 199] For example Seitz and de Fontaine (1978)[186] have used the model to do energy calculations for various arrangements of a pair of precipitates in Al-Cu alloys; the results indicated a tendency for the precipitates to stack as parallel disks, providing a possible explanation of the oberved behaviour of supersaturated Al-Cu solid solutions.

Diffusion can be represented in this model by allowing atoms of the two different kinds to exchange places from time to time, though sufficiently rarely to allow the lattice to come to equilibrium under the new forces after each exchange. These exchanges can be simulated by the Monte Carlo method known as Kawasaki dynamics, in which the following sequence of steps is carried out a large number of times: (i) choose a pair of neighbouring atoms at random, and also a random number ξ uniformly distributed between 0 and 1, (ii) calculate the increase in free energy ΔF that would occur if the two atoms were exchanged, and (iii) carry out the exchange if and only if $\xi < p(\Delta F)$, where the transition probability function $p(\cdot)$ is chosen so as to satisfy the detailed balance condition $p(x)/p(-x) = \exp(-x/\mathrm{k}T)$. The change in free energy consists of two parts: one is the change in (mean) energy which is equal to the change in the minimum potential energy as a function of the atomic displacements, since the vibrational energy is an unchanging $\mathrm{k}T$ per degree of freedom. The other part is an entropy term depending on the vibrational spectrum of the lattice, which is generally neglected. Indeed, this term is zero if the atomic stiffness parameters are independent of the way the two kinds of atoms are arranged on the lattice sites, a situation which makes the material elastically homogeneous. Just what part the entropy term should play in models capable of representing heterogeneous elasticity is unclear.

The harmonic approximation used in the Born model, though convenient, is not essential. In the simulations of Ikeda and Matsuda[77, 33] the microscopic potential energy function is represented as a sum of anharmonic two-body central forces and the energy, for a given arrangement of A and B atoms over the lattice sites, is then computed by numerical minimization over displacements, using a relaxation procedure. This method appears to be slower than the ones based on the harmonic approximation, but it has the potential advantage of greater realism.

We shall describe two types of simulation in which Kawasaki dynamics has been used to follow the diffusive motion of the atoms; one using central forces and heterogeneous elasticity, and the other using non-central forces and homogeneous elasticity.

5.2. Central Forces

5.2.1. The Model. In two dimensions, the elastic stiffness tensor of any crystal with hexagonal symmetry is isotropic; moreover, if only central forces act there is a Cauchy relation connecting the elastic constants which is[194] equivalent to $\nu = 1/4$ (ν = Poisson's ratio). In three dimensions, the elastic stiffness tensor of a harmonic crystal with fcc symmetry and only

central forces is likewise isotropic[20] and again Poisson's ratio is 1/4. Lee[53, 20] took advantage of these circumstances to simulate inclusions in a isotropic matrix using an atomic lattice model. He took the elastic energy to be the sum of the energies of a set of longitudinal harmonic springs, one for each pair of nearest neighbour sites, and both the stiffness and the natural length of each spring depended on the nature of the atoms at its two ends. In symbols, the elastic energy is

$$W = \tfrac{1}{4} \sum_{\mathbf{p}} \sum_{\mathbf{p}'} L(\mathbf{p}-\mathbf{p}', \gamma_{\mathbf{p}}, \gamma_{\mathbf{p}'})(r_{\mathbf{p},\mathbf{p}'} - l(\mathbf{p}-\mathbf{p}', \gamma_{\mathbf{p}}, \gamma_{\mathbf{p}'}))^2 \qquad (102)$$

where sums go over all the sites on some lattice, $\gamma_{\mathbf{p}}$ is defined to to be $+1$ if site $\mathbf{p}$ is occupied by an A atom and -1 if it is occupied by a B atom, $L(\mathbf{p}-\mathbf{p}', \gamma, \gamma')$ and $l(\mathbf{p}-\mathbf{p}', \gamma, \gamma')$ are the stiffness and natural length of the spring connecting an atom of type γ at site $\mathbf{p}$ to an atom of type γ' at site $\mathbf{p}'$, and $r_{\mathbf{p},\mathbf{p}'} = |\mathbf{x}_{\mathbf{p}} - \mathbf{x}_{\mathbf{p}'}| + (\mathbf{u}_{\mathbf{p}} - \mathbf{u}_{\mathbf{p}'}) \cdot (\mathbf{x}_{\mathbf{p}} - \mathbf{x}_{\mathbf{p}'})$ is the linearized distance between the atoms at sites $\mathbf{p}$ and $\mathbf{p}'$.

5.2.2. The Results. For a system of two inclusions in two dimensions, Lee found[53] that if the inclusions were softer than the matrix they deformed and eventually coalesced; if they were harder, they remained circular and the larger one grew while the smaller one shrank to zero. This work was extended to anisotropic elasticity in ref. 35, with similar results.

In ref. 20 Lee (1997) studies the effect of elastic inhomogeneity on a system of two inclusions for which the misfit strain and the elastic constants can both be different. If one inclusion is hard (i.e., harder than the matrix) and has a misfit strain while the other is soft and has no misfit, or a misfit of the opposite sign, then at equilibrium (in two dimensions) the soft inclusion surrounds the hard one. But if the soft inclusion has a misfit strain and the hard inclusion has none, the inclusions move away from one another; and if the two inclusions have misfit strains of the same sign, the soft inclusion partially wets the hard one but the rest of the soft inclusion tries to get away. Similar results are obtained in three dimensions. If an external stress is applied then the inclusions change their shape in a way compatible with Eq. (55). Reviews of this work, and more, are given in refs. 21 and 7.

Ikeda and Matsuda[77, 33] report on three dimensional simulations of a non-harmonic model. If the precipitates are elastically softer than the matrix, a giant percolating cluster forms (as in the diffuse-interface simulations described in Section 4.3.2 above). If the precipitates are as hard as the matrix, or harder, an ordered structure develops.

5.3. Noncentral Forces

5.3.1. The Model. Fratzl and Penrose (1994)[47] describe a model for use in atomic lattice simulations which is intended to represent coarsening in a cubic crystal with realistic elastic constants. For reasons explained earlier in this chapter, it is essential to include some non-central forces in the model. This can done by adding to the right side of the "longitudinal" elastic energy formula (102) a term representing transverse springs

$$\tfrac{1}{4}\sum_{\mathbf{p}}\sum_{\mathbf{p}'} T(\mathbf{p}-\mathbf{p}')\{(\mathbf{u}_{\mathbf{p}}-\mathbf{u}_{\mathbf{p}'})\wedge(\mathbf{x}_{\mathbf{p}}-\mathbf{x}_{\mathbf{p}'})/|\mathbf{x}_{\mathbf{p}}-\mathbf{x}_{\mathbf{p}'}|\}^2 \tag{103}$$

In these simulations, a square lattice was used, with elastic forces which can be pictured by imagining the atoms connected by three different types of spring: longitudinal springs connecting nearest neighbors, transverse springs connecting nearest neighbors, and longitudinal springs connecting next-nearest neighbours. To model the elastic misfit, the natural length of a longitudinal spring connecting sites $\mathbf{p}$ and $\mathbf{p}'$ was made to depend linearly on $\gamma_{\mathbf{p}}+\gamma_{\mathbf{p}'}$, but the stiffnesses of all the springs were taken to be independent of what type of atoms they connected. This model is characterized by three stiffness constants, the same as the number of elastic constants in a cubic crystal. It is possible, in fact, to relate the microscopic stiffnesses to the macroscopic elastic constants. Formulae for different lattices are given in, for example, refs. 205, 170, 47.

Given any configuration $\{\gamma_{\mathbf{p}}\}$ of A and B atoms on the lattice, the minimum of the elastic energy with respect to the atomic displacements $\mathbf{u}$ can be written down as a function of the $\gamma_{\mathbf{p}}$'s. The elastic free energy differs from this minimum by a constant, which can be ignored. Since the elastic constants are taken to be homogeneous, this calculation can be done using Fourier transforms,[205, 170] in a similar way to the derivation of Khachaturyan's formula (36) given in Section 2.1.3 (Eqs. (28)–(37)). The result can be written

$$W=\frac{1}{2N}\sum_{\mathbf{k}\neq 0}\mathsf{B}(\mathbf{k})\,|\tilde{\gamma}(\mathbf{k})|^2+\text{const.} \tag{104}$$

where the sum extends over the first Brillouin zone of the lattice and $\tilde{\gamma}$ is the Fourier transform of $\gamma_{\mathbf{p}}$:

$$\tilde{\gamma}(\mathbf{k})=\sum_{\mathbf{p}}\gamma_{\mathbf{p}}e^{i\mathbf{p}\cdot\mathbf{k}} \tag{105}$$

The "elastic potential" $\mathsf{B}(\mathbf{k})$ can be calculated for any type of lattice, and has been given explicitly for some, e.g., in refs. 205, 47.

The elastic energy (104) can be written in an alternative form, as a sum of interactions between pairs of lattice sites analogous to the double sum in Eq. (92). Adding to it the chemical energy, the important part of which can also be expressed as such a sum, we obtain for the total free energy

$$F = W_0 + \tfrac{1}{2} \sum_{\mathbf{p}} \sum_{\mathbf{p}'} (V_{el}(\mathbf{p}-\mathbf{p}') + V_{chem}(\mathbf{p}-\mathbf{p}'))\, \gamma_{\mathbf{p}} \gamma'_{\mathbf{p}} \tag{106}$$

where W_0 is a constant, $V_{el}(\mathbf{p})$ is the inverse Fourier transform of $\mathsf{B}(\mathbf{k})$ (in which we take $\mathsf{B}(\mathbf{0}) = 0$, so that $\sum_{\mathbf{p}} V_{el}(\mathbf{p}) = 0$) and $V_{chem}(\mathbf{p}-\mathbf{p}')\, \gamma_{\mathbf{p}} \gamma_{\mathbf{p}'}$ represents the short-range chemical interaction between two atoms on sites $\mathbf{p}$ and $\mathbf{p}'$.

The effects of external stress can also be treated to some extent within this framework.[52, 19] The treatment requires, however, a modification of the model since according to Eshelby's theorem (see Section 2.1.4) no effect will be seen for homogeneous elasticity. This modification is to assume that the stiffnesses of the springs depend weakly on what kind of atom they connect, and to treat the nonuniformity as a perturbation—for details see ref. 19. In analogy with the analysis for an elastic medium summarized at the end of Section 2.1.3, the elastic energy can be expressed as the sum of three parts, one of which is the non-quadratic "Eshelby" interaction. To keep the problem mathematically simple, this non-quadratic interaction was neglected in ref. 19.

5.3.2. The Results. The model just described can be used for simulations in various ways.

When the chemical interaction is taken to be a nearest-neighbour attraction and the elasticity has cubic anisotropy, stripe-like domains develop under the influence of the lattice misfit.[30] The stronger the misfit or the stronger the anisotropy of the elastic constants, the faster the anisotropy of the precipitates increases. The mean domain size, however, (defined as the ratio of area to perimeter) always increases in proportion to $t^{1/3}$ as in the case without elastic misfits.[30]

When uniaxial external stress is included in the model, wavy parallel stripes develop with an orientation depending on the direction of the applied stress.[52, 19] Thus, the cubic symmetry in the domain morphology is broken, in agreement with the experiments on rafting described in Section 1.2.3. Surprisingly, the mean domain size still increased in proportion to $t^{1/3}$.

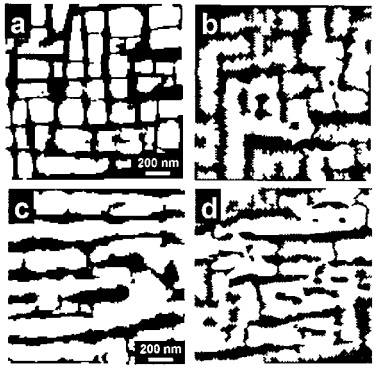

Fig. 8. (a) and (c) are reproductions of Figs. 1(e) and 1(g), respectively. (b) shows results from computer simulations of an Ising model with elastic interactions on a simple square lattice and with repulsive interaction of like atoms on nearest neighbor sites (with interaction energy J) and attractive interaction of like atoms on next nearest neighbor sites (energy J/2). Black shows the disordered phase (containing mostly A-atoms) and white the ordered phase (consisting of about half A and half B atoms). The overall concentration of B-atoms was 0.35 and the run was performed at a temperature of $T = 0.567$ J/k on a 128×128 lattice and stopped after 10^6 MCS. (d) The same model, temperature and annealing time as in (b), but with an additional external load along the vertical direction (simulations from ref. 14).

When the chemical interaction is taken to be a nearest neighbour repulsion instead of an attraction,[14] precipitates with atomic order of antiferromagnetic type are formed. The qualitatively new feature compared to the previous cases is that the precipitates can be ordered on two different atomic sublattices. Where two domains ordered on different sublattices meet, there is an anti-phase boundary (APB). Such APBs have the property of being wetted by the disordered matrix, thereby creating new boundaries between precipitates. The presence of wetted APBs also influences the rate of coarsening. The resulting patterns, illustrated in Fig. 8, are extremely similar to those found for nickel-base superalloys, as described in Section 1.21.[52, 19, 27, 99, 70, 36]

6. CONCLUSION

We can now consider to what extent the theoretical models we have been describing explain the various experimental phenomena mentioned in Section 1.2.

6.1. The Shapes of the Precipitates

The plate-like shape of the individual precipitates in alloys such as Al-Cu and Cu-Be, mentioned in Section 1.2.1, is consistent with the predic-

tion of the sharp-interface model (Section 2.3.1) that when the interface energy is negligible and the material is elastically anisotropic the equilibrium shapes of the precipitates are plates perpendicular to an elastically soft direction. Two-dimensional multi-precipitate simulations with anisotropic elasticity, using either the diffuse-interface model (see Section 4.3.2 and Fig. 7(d,e)) or the atomic lattice model,[30] also give long thin precipitates perpendicular to an elastically soft direction.

The dependence of the shape of precipitates on their size, (more precisely, on the parameter R/R_0 defined in Section 1.1) was investigated in the experiments with Ni-Al-Mo alloys illustrated in Fig. 1. The individual precipitates looked round when this parameter was very small, but roughly square when it was large. All three of the models we have described explain this dependence as an effect of the elastic anisotropy; it is seen particularly clearly in calculations using the sharp interface and diffuse interface models, where the behaviour of a single precipitate as a function of its size (that is, of the ratio of its elastic to its interfacial energy) has been considered (see Sections 2.3.1, 3.2.2 and 4.3.1).

The splitting of large cube-like precipitates in some nickel-base alloys (see Fig. 4) has also been investigated using various theoretical approaches, but the results are inconsistent. Sharp-interface energy calculations assuming inclusions of fixed shape do give this effect (Sections 2.3.1 and 2.3.2), as do diffuse-interface calculations of the equilibrium shape (Section 4.3.1). On the other hand the sharp-interface evolution calculations that have been done so far (Section 3.2.2) do not exhibit the effect—possibly because of the difficulty of following topological changes in the sharp-interface model.

6.2. The Arrangement of the Precipitates

Experiments show that when the (anisotropic) elastic interaction is strong enough to affect the shapes of the precipitates, these precipitates tend to align along certain directions (see Fig. 1(c)). A similar type of ordering is found in the sharp-interface model (Sections 2.3.3, 3.2.3, 3.2.4) and the diffuse-interface model (Section 4.3.2).

6.3. The Rate of Coarsening

While the $t^{1/3}$ growth law for coarsening in alloys without elastic misfit is reasonably well understood,[225, 226, 133] theory has been less successful in explaining the time-dependence when elastic forces do act. The experiments illustrated in Fig. 3 indicate[55] that if the elasticity is strongly anisotropic and (relatively) weakly heterogeneous, the coarsening follows a $t^{1/3}$ growth

law, whereas if it is weakly anisotropic and strongly heterogeneous, the coarsening follows a $t^{1/3}$ law only for a limited time, and then slows down or stops. The atomic lattice simulations described in Section 5.3.2 also give $t^{1/3}$ growth for an elastically homogeneous anisotropic lattice, but theory does not explain why the elastic forces apparently do not affect the growth exponent at all in this case. For a heterogeneous lattice without anisotropy the diffuse-interface simulations described in Section 4.3.2 predicted that the growth would be slower than $t^{1/3}$ but not that the growth exponent would change rather abruptly as shown in Fig. 3(b,c). Theory also predicts an interesting topological rearrangement if in the initial configuration the precipitates are softer (less rigid) than the matrix, but these experiments did not reveal any striking difference of behaviour between precipitates that were much softer than the matrix and ones that were harder.

6.4. Rafting

The effect of an externally applied stress on the shapes and arrangement of the precipitates, described in Section 1.2.3 and illustrated in Fig. 1(g), can be understood in principle on the basis of isotropic (but inhomogeneous) elasticity using the sharp interface model, as discussed in Section 2.2.1. The effect has been studied in a more detailed way, both for isotropic and anisotropic elasticity, using all three of the theoretical approaches we have described (Sections 2.2.2, 4.3.2, 5.2.2, 5.3.2 and Fig. 8(c,d)). All these approaches reproduce, to a greater or less extent, the qualitative experimental features of rafting, summarized in equation (55).

6.5. Generalizations of the Model

Figures 2 and 8 illustrate two cases that go beyond the simple binary alloy with either isotropic or homogeneous anisotropic elasticity which underlies most of the theoretical work described in this article. In Fig. 2 the precipitates have a different crystal symmetry from the matrix, and in Fig. 8 the precipitates can occur in more than one variant. In both cases, the results illustrate the excellent qualitative agreement with experiment that simulations based on a well-chosen theoretical model can give.

APPENDIX. LIST OF SYMBOLS

Symbol	First appearance	Meaning
$B(\mathbf{k})$	(37)	
$\mathsf{B}(\mathbf{k})$	(104)	"elastic potential"
C_{11}, C_{12}, C_{44}	(7)	elastic moduli of cubic crystal

c	(57)	concentration of A (solute) atoms
c_0^α	Section 3.1	zero-temperature equilbrium value of c in Ω_α
c_0	(95)	concentration at which stress-free strain is 0
D	(57)	diffusivity
E	(39)	Young's modulus
e_{ij}	(3)	strain tensor
e_{ij}^0	(4)	stress-free strain tensor
e_{ij}^{ext}	(31)	"externally applied strain"
e_{ij}^α	(34)	stress-free strain in phase α
F	(2)	free energy of system
F^Γ	(2)	free energy of interface
f	(2)	thermodynamic free energy density
G	(6)	shear modulus
H_{ijmn}	(38)	
K	(6)	bulk modulus
K_*, $K_\bullet$	(45), (53)	
k		Boltzmann's constant
L	(102)	stiffness of a longitudinal spring
l	(102)	natural length of a longitudinal spring
M	(80, 94)	mobility coefficient or matrix
$\mathbf{n}$	various	a unit vector
p	(27)	excess pressure inside inclusion
$\mathbf{p}$	(92)	a lattice site
q	(4)	isotropic stress-free strain
R	Section 1.1	radius of (spherical) precipitate
R_0	Section 1.1	"crossover" value of R
$r_{\mathbf{p},\mathbf{p}'}$	(102)	linearized distance between atoms on sites $\mathbf{p}$, $\mathbf{p}'$
T		temperature
T	(103)	stiffness of a transverse spring
T_0	(79)	mean-field transition temperature
$\mathbf{u}$	(3)	displacement field
$\mathbf{u}'$	(18)	periodic part of $\mathbf{u}$
V	(93)	total effective two-site interaction
V_{chem}	(106)	chemical interaction
V_{el}	(90)	two-point elastic interaction
v_n	(58)	normal velocity of interface
W		elastic energy of the specimen
W^{ext}	(2)	potential energy of loading mechanism
W_{int}	(56)	elastic interaction energy
w	(2)	elastic energy density
$\bar{w}_\alpha$	(44)	space average of w
$\mathbf{x}$	(2)	reference position of material point
x_i	(3)	Cartesian components of $\mathbf{x}$ $(i=1, 2, 3)$
Z	(33)	
α, β		the A-rich, B-rich phases
Γ	(2)	the interface between phases α and β
γ	(102)	$+1$ (-1) for site occupied by an A (B) atom
$\Delta(\mathbf{z})$	(93)	χ times finite-difference Laplacian
$(\Delta e)_{ij}$	(6)	$e_{ij}-e_{ij}^0$
δ_{ij}	(4)	1 if $i=j$, 0 if not

η	(95)	compositional expansion coefficient
$\eta(\mathbf{x})$	(84)	order-parameter field
$\theta(\mathbf{k})$	(35)	
κ	(26)	mean curvature of Γ
Λ	(84)	kinetic coefficient in Allen–Cahn equation
λ_{ijmn}	(5)	elastic (stiffness) tensor
μ	(60)	chemical potential
$\hat{\mu}$	(87)	diffusion potential
ν	(39)	Poisson's ratio
π	(63)	grand canonical pressure
σ	(8)	interfacial energy (surface tension)
χ	(78)	coefficient of gradient term in free energy density
Ψ_{ijmn}	(32)	
$\Omega, \Omega_\alpha, \Omega_\beta$	(2)	region occupied by specimen, inclusions, matrix
$\partial\Omega$	(9)	surface of Ω
$\lvert\Omega\rvert$	(30)	volume of Ω

ACKNOWLEDGMENTS

We thank Istvan Gyöngy, Armen Khachaturyan and Peter Voorhees for helpful information and suggestions, Richard Weinkamer for his comments on an earlier draft of this paper, and the Austrian Academy of Sciences for financial support.

REFERENCES

1. Y. Le Bouar, A. Loiseau, and A. G. Khachaturyan, Origin of chessboard-like structures in decomposing alloys. Theoretical model and computer simulations, *Acta Mater.* **46**:2777–2788 (1998).
2. L. Q. Chen and L. J. Shen, Applications of semi-implicit Fourier-spectral method to phase-field equations, *Computer Physics Commun.* **108**:147–158 (1998).
3. M. E. Gurtin and P. W. Voorhees, On the effects of elastic stress on the motion of fully faceted interfaces, *Acta Mater.* **46**:2103–2112 (1998).
4. J. E. Guyer and P. W. Voorhees, Morphological stability and compositional uniformity of alloy thin films, *J. Crystal Growth* **187**:150–165 (1998).
5. I. Gyöngy, private communication (1998).
6. T. Koyama and T. Miyazaki, Computer simulation of phase decomposition in two dimensions based on a discrete type non-linear diffusion equation, *Materials Transactions JIM* **39**:169–178 (1998).
7. J. K. Lee, Elastic stress and microstructural evolution, *Materials Transactions JIM* **39**:114–132 (1998).
8. P. H. Leo, J. S. Lowengrub and H. J. Jou, A diffuse interface model for microstructural evolution in elastically stressed solids, *Acta Mater.* **46**:2113–2130 (1998).
9. F. Léonard and R. C. Desai, Alloy decomposition and surface instabilities in thin films, *Phys. Rev. B* **57**:4805–4815 (1998).
10. D. Y. Li and L. Q. Chen, Morphological evolution of coherent multivariant $Ti_{11}Ni_{14}$ precipitiates in Ti-Ni alloys under an applied stress—a computer simulation study, *Acta Mater.* **46**:639–649 (1998).

11. D. Y. Li and L. Q. Chen, Computer simulation of stress-oriented nucleation and growth of theta′ precipitates in Al-Cu alloys, *Acta Mater.* **46**:2573–2585 (1998).
12. A. M. Mebed and T. Miyazaki, *Metall. and Mater. Trans. A* **29**:739–749 (1998). Computer simulation and experimental investigation of the spinodal decomposition in the beta Ti-Cr binary alloy system.
13. R. Mueller and D. Gross, The 3-D simulation of equilibrium morphologies of precipitates, *Comp. Mater. Sci.* **11**:35–44 (1998).
14. P. Nielaba, P. Fratzl, and J. L. Lebowitz, Growth of ordered domains in a computer model with lattice misfit: to appear in *J. Stat. Phys.*
15. I. Schmidt, R. Mueller, and D. Gross, The effect of elastic inhomogeneity on equilibrium and stability of a two particle morphology, *Mechanics of Materials* **30**:181–196 (1998).
16. Y. Wang, D. Banarjee, C. C. Su, and A. G. Khachaturyan, Field kinetic model and computer simulation of ordered intermetallics from FCC solid solutions, *Acta Mater.* **46**:2983–3001 (1998).
17. J.-H. Cho and A. J. Ardell, Coarsening of Ni_3-Si precipitates in binary Ni-Si alloys at intermediate and large volume fractions, *Acta Mater.* **45**:1393–1400 (1997).
18. H. J. Jou, P. H. Leo, and J. S. Lowengrub, Microstructural evolution in inhomogeneous elastic media, *J. Comp. Phys.* **131**:109–148 (1997).
19. C. A. Laberge, P. Fratzl, and J. L. Lebowitz, Microscopic model for directional coarsening of precipitates in alloys under external load, *Acta Mater.* **45**:3949–3961 (1997).
20. J. K. Lee, Morphology of coherent precipitates via a discrete atom method, *Mater. Sci and Eng. A* **238**:1–12 (1997).
21. J. K. Lee, Studying stress-induced morphological evolution with the discrete atom method, *JOM—Journal of the Minerals, Metals and Materials Society* **49**:37 (1997).
22. A. Malik, B. Schönfeld, G. Kostorz, W. Bührer, and J. S. Pedersen, Early stages of decomposition in Al-Ag and Al-Cu, *Z. Metallkde* **88**:625–629 (1997).
23. T. Ohashi, K. Hidaka, and S. Imano, Elastic stress in single-crystal Ni-base superalloys and the driving force for their microstructural evolution under high-temperature creep conditions, *Acta Mater.* **45**:1801–1810 (1997).
24. O. Paris, M. Fährmann, E. Fährmann, T. M. Pollock, and P. Fratzl, Early stages of precipitate rafting in a single crystal Ni-Al-Mo alloy investigated by small-angle X-ray scattering and TEM, *Acta Mater.* **45**:1085–1097 (1997).
25. I. Schmidt and D Gross, The equilibrium shape of an elastically inhomogeneous inclusion, *J. Mech. Phys. Solids* **45**:1521–1549 (1997).
26. M. E. Thompson and P. W. Voorhees, Spinodal decomposition in elastically anisotropic homogeneous systems in the presence of an applied traction, *Modelling and Simulation in Mater. Sci. and Eng.* **5**:223–243 (1997).
27. M. Véron and P. Bastie, Strain induced directional coarsening in nickel-based superalloys: investigation on kinetics using the small angle neutron scattering (SANS) technique, *Acta Mater.* **45**:3277–3282 (1997).
28. P. Vyskocil, J. Skov Pedersen, G. Kostorz, and B. Schönfeld, Small-angle neutron scattering of precipitates in Ni-Ti alloys—I. Metastable states in poly- and single crystals, *Acta Mater.* **45**:3311–3318 (1997).
29. Y. Wang and A. G. Khachaturyan, Three-dimensional field model and computer modeling of martensitic transformations, *Acta Materialia* **45**:759–773 (1997).
30. P. Fratzl and O. Penrose, Ising model for phase separation in alloys with anisotropic elastic interaction—II. A computer experiment, *Acta Mater.* **44**:3227–3239 (1996).
31. J. E. Guyer and P. W. Voorhees, Morphological instability of alloys and thin films, *Phys Rev. B* **54**:11710–11724 (1996).

32. W. Hort and W. C. Johnson, Effect of uniaxial stress on coarsening of precipitate clusters, *Met. and Mater. Trans.* **27A**:1461–1476 (1996).
33. H. Ikeda and H. Matsuda, Computer simulation of phase decomposition process generating precipitates harder than matrix, *Mater. Trans. JIM* **37**:1413–1421 (1996).
34. M. Kato, T. Fujii, and S. Onaka, Elastic strain energies of sphere, plate and needle inclusions, *Mater. Sci and Eng. A—Structural Materials* **211**:95–103 (1996).
35. J. K. Lee, A study on coherent strain and precipitate morphology via a discrete atom method, *Metall. and Mater. Trans.* **27A**:1449–1459 (1996).
36. F. R. N. Nabarro, C. M. Cress, and P. Kotschy, The thermodynamic driving force for rafting in superalloys, *Acta Mater.* **44**:3189–3198 (1996).
37. F. R. N. Nabarro, Inclusions and inhomogeneities under stress, *Phil. Mag. Lett.* **73**:45–49 (1996).
38. G. Sauthoff, Influences of stresses on precipitation, *Jour. de Physique IV* **6(C1)**:87–97 (1996).
39. C. H. Su and P. W. Voorhees, The dynamics of precipitate evolution in elastically stressed solids—I. Inverse coarsening, *Acta Mater.* **44**:1987–2000 (1996).
40. C. H. Su and P. W. Voorhees, The dynamics of precipitate evolution in elastically stressed solids—II. Particle alignment, *Acta Mater.* **44**:2001–2016 (1996).
41. J. Svoboda and P. Lukáč, Modeling of kinetics of directional coarsening in Ni-superalloys, *Acta Mater.* **44**:2557–2565 (1996).
42. Y. Z. Wang, L. Q. Chen, and A. G. Khachaturyan, Three-dimensional dynamic simulation of the equilibrium shape of a coherent tetragonal precipitate in Mg-partially stabilized cubic ZrO_2, *J. Amer. Ceramic Soc.* **79**:987–991 (1996).
43. T. A. Abinandanan and W. C. Johnson, Development of spatial correlations during coarsening, *Mat. Sci. Eng. B* **32**:169–176 (1995).
44. J. Y. Buffière and M. Ignat, A dislocation based criterion for the raft formation in nickel-based superalloy single crystals, *Acta Metall. Mater.* **43**:1791–1797 (1995).
45. J. W. Cahn and R. Kobayashi, Exponentially rapid coarsening and buckling in coherently self-stressed thin plates, *Acta Met. Mater.* **43**:931–944 (1995).
46. M. Fährmann, P. Fratzl, O. Paris, E. Fährmann, and W. C. Johnson, Influence of coherency stress on microstructural evolution in model Ni-Al-Mo alloys, *Acta Metall. Mater.* **43**:1007 (1995).
47. P. Fratzl and O. Penrose, Ising model for phase separation in alloys with anisotropic elastic interactions—I. Theory, *Acta Metall. Mater.* **43**:2921–2930 (1995).
48. V. Gröger, P. Fratzl, W. Pahl, O. Paris, G. Bischof, and G. Krexner, Phase boundary structure of γ'-particles in Cu-10 at % Be, *Acta Metall. Mater.* **43**:1305–1311 (1995).
49. J. E. Guyer and P. W. Voorhees, Morphological stability of alloys and thin films, *Phys. Rev. Letters* **74**:4031–4034 (1995).
50. A. G. Khachaturyan, S. Semenovskaya, and T. Tsakalakos, Elastic strain energy of inhomogeneous solids, *Phys. Rev. B* **52**:15909–15919 (1995).
51. T. Koyama, T. Miyazaki, and A. E. Mebed, Computer simulations of phase decomposition in real alloy systems based on the modified Khachaturyan diffusion equation, *Metal. Mater. Trans. A* **26**:2617–2623 (1995).
52. C. A. Laberge, P. Fratzl, and J. L. Lebowitz, Elastic effects on phase segregation in alloys with external stresses, *Phys. Rev. Lett.* **75**:4448–4451 (1995).
53. J. K. Lee, Coherence strain analysis via a discrete atom method, *Scripta Met. et Mat.* **32**:559–564 (1995).
54. O. Paris, M. Fährmann, and P. Fratzl, Breaking of rotational symmetry during decomposition of elastically anisotropic alloys, *Phys. Rev. Lett.* **75**:3458–3461 (1995).

55. O. Paris, F. Langmayr, G. Vogl, and P. Fratzl, A possible criterion for slowing down of precipitate coarsening due to elastic misfit interactions, *Z. Metallkd.* **86**:860 (1995).
56. I. Schmidt and D. Gross, A strategy for determining the equilibrium shape of an inclusion, *Arch. Mech.* **47**:379–390 (1995).
57. A. D. Sequiera, H. A. Calderon, G. Kostorz, and J. S. Pedersen, Bimodal size distribution of γ' precipitates in Ni-Al-Mo—I. Small-angle neutron scattering, *Acta Metall. Mater.* **43**:3427–3439 (1995).
58. A. D. Sequiera, H. A. Calderon, G. Kostorz, and J. S. Pedersen, Bimodal size distribution of γ' precipitates in Ni-Al-Mo—II. Transmission electron microscopy, *Acta Metall. Mater.* **43**:3441–3451 (1995).
59. K.-I. Udoh, A. M. El Araby, Y. Tanaka, K. Hisatsune, K. Yasuda, G. van Tendeloo, and J. van Landuyt, Structural aspects of AuCu I or AuCu II and a cuboidal block configuration of f.c.c. disordered phase in Au-Cu-Pt and AuCu-Ag, *Mater. Sci. Eng. A* **203**:154–164 (1995).
60. Y. Wang and A. G. Khachaturyan, Shape instablity during precipitate growth in coherent solids, *Acta Metall. Mater.* **43**:1837–1857 (1995).
61. Y. Z. Wang, H. Y. Wang, L. Q. Chen, and A. G. Khachaturyan, Microstructural development of coherent tetragonal precipitates in magnesium-partially stabilized zirconia—a computer simulation, *J. Amer. Ceramic Soc.* **78**:657–661 (1995).
62. Y. Wang and A. G. Khachaturyan, Microstructural evolution during the precipitation of ordered intermetallics in multiparticle coherent systems, *Phil. Mag. A* **72**:1161–1171 (1995).
63. N. D. Alikakos, P. W. Bates, and X. F. Chen, Convergence of the Cahn–Hilliard equation to the Hele-Shaw model, *Arch. Rat. Mech. Anal.* **128**:165–205 (1994).
64. D. J. Arrell and J. L. Vallés, Interfacial dislocation based criterion for the prediction of rafting behavior in superalloys, *Scripta Metall. Mater.* **30**:149–53 (1994).
65. P. Fratzl and O. Paris, Internal oxidation of Cu-Fe. II. The morphology of oxide inclusions from the minimization of elastic misfit energy, *Acta Metall. Mater.* **42**:2027–2033 (1994).
66. W. Hort and W. C. Johnson, Diffusional boundary conditions during coarsening of elastically interacting precipitates, *Metall and Met. Trans. A* **25**:2695–2703 (1994).
67. F. Langmayr, P. Fratzl, and G. Vogl, Crossover from ω-phase to α-phase precipitation in bcc Ti-Mo, *Phys. Rev. B* **49**:11759–11766 (1994).
68. G. Muralidharan, J. E. Epperson, M. Petri, and Haydn Chen, Coherency strains and coarsening in Ni-Al-Si alloys: an experimental study, *Solid-Solid Phase Transformations*, W. C. Johnson, J. M. Howe, D. E. Laughlin, and M. A. Soffa, eds. (The Minerals, Metals & Materials Society, 1994).
69. O. Paris, P. Fratzl, F. Langmayr, G. Vogl, and H. G. Haubold, Internal oxidation of Cu-Fe. I. Small-angle X-ray scattering study of oxide precipitation, *Acta Metall. Mater.* **42**:2019–2026 (1994).
70. T. M. Pollock and A. S. Argon, Directional coarsening in nickel-base single crystals with high volume fractions of coherent precipitates, *Acta Metall. Mater.* **42**:1859–1874 (1994).
71. Y. Y. Qu, H. A. Calderon, and G. Kostorz, Coarsening of coherent γ'-precipitates in a Ni-Al-Mo alloy, *Solid-Solid Phase Transformations*, W. C. Johnson, J. M. Howe, D. E. Laughlin, and W. A. Soffa, eds. (The Minerals, Metals & Materials Society, 1994).
72. C. Sagui, A. M. Somoza, and R. Desai, Spinodal decomposition in an order-disorder phase transition with elastic fields, *Phys. Rev. E* **50**:4865–4879 (1994).
73. M. E. Thompson, C. S. Su, and P. W. Voorhees, The equilibrium shape of a misfitting precipitate, *Acta Metall.* **42**:2107–2122 (1994).

74. J. L. Vallés and D. J. Arrell, Monte Carlo simulation of anisotropic coarsening in nickel-base superalloys, *Acta Metall. Mater.* **42**:2999–3008 (1994).
75. T. A. Abinandanan and W. C. Johnson, Coarsening of elastically interacting coherent particles—I. Theoretical formulation, *Acta Metall. Mater.* **41**:17–25 (1993).
76. T. A. Abinandanan and W. C. Johnson, Coarsening of elastically interacting coherent particles—II. Simulations of preferential coarsening and particle migrations, *Acta Metall. Mater.* **41**:27–39 (1993).
77. H. Ikeda and H. Matsuda, Effects of differences of elastic moduli between constituents on spinodal decomposition processes, *Mater. Trans. JIM* **34**:651–657 (1993).
78. P. H. Leo and H. J. Jou, Shape evolution of an initially circular precipitate growing by diffusion in an applied stress field, *Acta Metall. Mater.* **41**:2271–2281 (1993).
79. A. Maheshwari and A. J. Ardell, Morphological evolution of coherent misfitting precipitates in anisotropic elastic media, *Phys. Rev. Lett.* **70**:2305–2308 (1993).
80. T. Miyazaki and T. Koyama, Stability against coarsening in elastically constrained many-particle systems, *Mater. Sci and Eng. A* **169**:159–65 (1993).
81. S. Nambu and A. Sato, Elastic effect on domain morphology and kinetics of spinodal decomposition in the tetragonal system, *J. Amer. Ceramic Soc.* **76**:1978–84 (1993).
82. S. Socrate and D. M. Parks, Numerical determination of the elastic driving force for directional coarsening in Ni-superalloys, *Acta Metall. Mater.* **41**:2185–2209 (1993).
83. B. J. Spencer, P. W. Vorhees, and S. H. Davis, Morphological instability in epitaxially strained dislocation-free solid films—linear stability theory, *J. Appl. Phys.* **73**:4955–4970 (1993).
84. B. J. Spencer, S. H. Davis, and P. W. Voorhees, Morphological instability in epitaxially strained dislocation-free solid films—nonlinear evolution, *Phys. Rev. B* **47**:9760–9777 (1993).
85. Y. Wang, L.-Q. Chen, and A. G. Khachaturyan, Kinetics of strain-induced morphological transformations in cubic alloys with a miscibility gap, *Acta Met. Mat.* **41**:279–296 (1993).
86. M. Doi and T. Miyazaki, A new parameter for describing the structure bifurcation in two-phase alloys containing coherent precipitates, *J. Mater. Sci.* **27**:6291–6298 (1992).
87. W. C. Johnson and P. W. Voorhees, Elastically-induced precipitate shape transitions in coherent solids, *Solid State Phenomena* **23–24**:87–103 (1992).
88. W. C. Johnson and P. W. Voorhees. In *Nonlinear Phenomena in Materials Science*, G. Martin and L. Kubin, eds. (Trans Tech, Clauthal, Germany, 1992).
89. F. C. Larché and J. W. Cahn, Phase changes in a thin plate with nonlocal self-stress effects, *Acta Met. Mater.* **40**:947–955 (1992).
90. M. McCormack, A. G. Khachaturyan, and J. W. Morris, Jr., A two-dimensional analysis of the evolution of precipitates in elastic media, *Acta Met. Mat.* **40**:325–336 (1992).
91. M. McCormack and J. W. Morris, Jr., Strain-induced shape shange of cubic preciptiates in a cubic matrix with positive anisotropy, *Acta Met. Mat.* **40**:2489–2945 (1992).
92. H. Nishimori and A. Onuki, Evolution of soft domains in two-phase alloys: shape changes, surface instability and network formation, *Phys. Lett. A* **162**:323–326 (1992).
93. R. Shneck, R. Alter, A. Brokman, and M. P. Daniel, Fundamentals of the anisotropy of elastic interactions between dilating particles in a cubic material, *Phil. Mag. A* **65**:797–814 (1992).
94. A. Takeuchi, T. Koyama, and T. Miyazaki, Computer simulation of the phase decomposition of Al-Zn and Fe-Mo alloys based on the nonlinear diffusion equation (in Japanese), *J. Japan Institute of Metals* **57**:492–500 (1993), see also *Mater. Sci. Eng. A* **169**:159–165 (1993).

95. P. W. Voorhees, G. B. McFadden, and W. C. Johnson, On the morphological development of second-phase particles in elastically stressed solids, *Acta Metall. Mater.* **40**:2979–2992 (1992).
96. P. W. Voorhees, Ostwald ripening of two-phase mixtures, *Ann Rev. Mat. Sci.* **22**:197–215 (1992).
97. Y. Wang, L. Q. Chen, and A. G. Khachaturyan, Particle translational motion and reverse coarsening phenomena in multiparticle systems induced by long-range elastic interactions, *Phys. Rev. B* **46**:11194–11197 (1992).
98. K. Binder, Spinodal decomposition. In *Materials science and technology*, P. Haasen, ed., Vol. 5, VCH (Weinheim, New York, 1991), p. 405.
99. J. C. Chang and S. M. Allen, Elastic energy changes accompanying γ' rafting in nickel-base superalloys, *J. Mater. Res.* **6**:1843–1855 (1991).
100. L.-Q. Chen and A. G. Khachaturyan, Computer simulation of structural transformations during precipitation of an ordered intermetallic phase, *Acta Met. Mater.* **39**:2533–2551 (1991).
101. L.-Q. Chen and A. G. Khachaturyan, *Scripta Met. Mater.* **25**:61–66 (1991).
102. P. Fratzl, J. L. Lebowitz, O. Penrose, and J. Amar, Scaling functions, self similarity, and the morphology of phase separating systems, *Phys. Rev. B* **44**:4794–4811 (1991).
103. C. Leroux, A. Loiseau, D. Broddin, and G. van Tendeloo, Electron microscopic study of the coherent two-phase mixtures $Ll_0 + Ll_1$ in Co-Pt alloys, *Phil. Mag. B* **64**:57–82 (1991).
104. H. Nishimori and A. Onuki, Freezing of domain growth in cubic solids with elastic misfit, *J. Phys. Soc. Japan* **60**:1208–1211 (1991).
105. A. Onuki and H. Nishimori, On Eshelby's elastic interaction in two-phase solids, *J. Phys. Soc. Japan* **60**:1–4 (1991).
106. A. Onuki, Interface motion in two-phase solids with elastic misfits, *J. Phys. Soc. Japan* **60**:345–348 (1991).
107. A. Onuki and H. Nishimori, Anomalously slow domain growth due to a modulus inhomogeneity in phase-separating alloys, *Phys. Rev. B* **43**:13649–13652 (1991).
108. O. Penrose, A mean-field equation for the dynamic Ising model, *J. Stat. Phys.* **63**:975–986 (1991).
109. B. J. Spencer, P. W. Voorhees, and S. H. Davis, Morphological instability in epitaxially strained dislocation-free solid films, *Phys. Rev. Lett.* **67**:3696–3699 (1991).
110. Y. Wang, L.-Q. Chen, and A. G. Khachaturyan, Shape evolution of a precipitate during strain-induced coarsening—a computer simulation, *Scripta Met. et Mat.* **25**:1387–1392 (1991).
111. Y. Wang, L.-Q. Chen, and A. G. Khachaturyan, Strain-induced modulated structures in two-phase cubic alloys, *Scripta Met. et Mat.* **25**:1969–1974 (1991).
112. H. Calderon and G. Kostorz, Lattice misfit and decomposition in Ni-Al-Mo alloys. In *Neutron Scattering in Materials Science*, S. M. Shapiro, S. C. Moss, and S. D. Jorgensen, eds., Mat. Res. Soc. Symp. Proc. 166, p. 255 (1990).
113. A. Cerri, B. Schönfeld, and G. Kostorz, Decomposition kinetics in Ni-Ti alloys, *Phys. Rev. B* **42**:958–960 (1990).
114. W. C. Johnson, T. A. Abinandanan, and P. W. Voorhees, The coarsening kinetics of two misfitting particles in an anisotropic crystal, *Acta Metall. Mater.* **38**:1349–1367 (1990).
115. P. H. Leo, W. W. Mullins, R. F. Sekerka, and J. Viñals, Effect of elasticity on late stage coarsening, *Acta Metal. Mater.* **38**:1573–1580 (1990).
116. H. Nishimori and A. Onuki, Pattern formation in phase separating alloys with cubic symmetry, *Phys. Rev. B* **42**:980–983 (1990).

117. A. Onuki. In *Formation, Dynamics and Statistics of Patterns*, K. Kawasaki, M. Suzuki and A. Onuki, eds. (World Scientific, Sinagapore, 1990).
118. B. Caroli, C. Caroli, B. Roulet, and P. W. Voorhees, Effect of elastic stresses on the morphological stability of a solid sphere growing from a supersaturated melt, *Acta Met.* **37**:257–268 (1989).
119. A. Chakrabarti, R. Torál, and J. D. Gunton, Late stages of spinodal decomposition in a three-dimensional model system, *Phys. Rev. B* **39**:4386–4394 (1989).
120. J. G. Conley, M. E. Fine, and J. R. Weertmann, Effect of lattice disregistry variation on the late stage phase transformation behavior of precipitates in Ni-Al-Mo alloys, *Acta Metall.* **37**:1251 (1989).
121. C. M. Elliott, pp. 35–74 of *Mathematical Models for Phase Change Problems*, J. Rodrigues, ed., Int. Ser. Num. Math. Vol. 88 (Birkhäuser, Stuttgart, 1989).
122. Y. Enomoto and K. Kawasaki, Computer simulation of Ostwald ripening with elastic field interactions, *Acta Metall.* **37**:1399–1406 (1989).
123. J. Gayda and D. J. Srolovitz, A Monte Carlo finite element model for strain energy controlled microstructural evolution: "Rafting" in superalloys, *Acta Metall.* **37**:641–650 (1989).
124. U. Glatzel and M. Feller-Kriepmayer, Calculations of internal stresses in the γ/γ' microstructure of a nickel-base superalloy with high volume fraction of the γ'-phase, *Scripta Metall.* **23**:1839–1844 (1989).
125. H. Hein, Nucleation, growth and coarsening in Ni-5.0 at % Al-5.8 at % Ti, *Acta Metall.* **37**:2145 (1989).
126. W. C. Johnson, P. W. Voorhees, and D. E. Zupon, The effects of elastic stress on the kinetics of Ostwald ripening: the two-particle problem, *Metall. Trans.* **20A**:1175 (1989).
127. I. M. Kaganova and A. L. Roitburd, An anisotropic crystalline inclusion in an isotropic matrix, *Sov. Phys. Crystall.* **34**:650–653 (1989) (English translation of *Kristalografia* **34**:1076–82 (1988)).
128. M. J. Kaufman, P. W. Voorhees, W. C. Johnson, and F. S. Biancaniello, An elastically induced morphological instability of a misfitting precipitate, *Metall. Trans. A* **20A**:2171–2175 (1989).
129. V. J. Laraia, W. C. Johnson, and P. W. Voorhees, Kinetics of Ostwald ripening in stressed solids—the low volume-fraction limit, *Scripta Met.* **23**:1749–1754 (1989).
130. P. H. Leo and R. F Sekerka, The effect of surface stress on crystal–melt and crystal–crystal equilibrium, *Acta Metall.* **37**:3119–3138 (1989).
131. P. H. Leo and R. F Sekerka, The effect of elastic fields on the morphological stability of a precipitate grown from solid solution, *Acta Metall.* **37**:3139–3149 (1989).
132. T. Miyazaki and M. Doi, Shape bifurcations in the coarsening of precipitates in elastically constrained systems, *Mat. Sci. Eng. A* **110**:175–185 (1989).
133. W. W. Mullins and J. Viñals, Self-similarity and growth kinetics driven by surface free energy reduction, *Acta Metall.* **37**:991–997 (1989).
134. A. Onuki, Ginzburg–Landau approach to elastic effects in the phase separation of solids, *J. Phys. Soc. Japan* **58**:3065–3068 (1989).
135. A. Onuki, Long-range interactions through elastic fields in phase-separating solids, *J. Phys. Soc. Japan* **58**:3069–3072 (1989).
136. R. L. Pego, Front migration in the nonlinear Cahn–Hilliard equation, *Proc. Roy. Soc. A* **422**:261–278 (1989).
137. D. J. Srolovitz, On the stability of surfaces of stressed solids, *Acta Metall.* **37**:621–625 (1989).
138. W. C. Johnson, M. B. Berkenpas, and D. E. Laughlin, Precipitate shape transitions during coarsening under uniaxial stress, *Acta Met.* **36**:3149–3162 (1988).

139. I. M. Kaganova and A. L. Roitburd, Equilibrium between elastically interacting phases, *Soviet Physics JETP* **67**:1173–1183 (1988).
140. K. Kawasaki and Y. Enomoto, Statistical theory of Ostwald ripening with elastic field interactions, *Physica A* **150**:463–498 (1988).
141. A. G. Khachaturyan, S. V. Semenovskaya, and J. W. Morris, Jr., Theoretical analysis of strain-induced shape changes in cubic precipitates during coarsening, *Acta Metall.* **36**:1563–1572 (1988).
142. V. J. Laraia, W. C. Johnson, and P. W. Voorhees, Growth of a coherent precipitate from a supersaturated solution, *J. Mater. Res.* **3**:257–266 (1988).
143. Y. Oono and S. Puri, Study of phase-separation dynamics by use of cell dynamical systems I. modelling, *Phys. Rev. A* **38**:434–453 (1988).
144. C. Rottman, P. W. Voorhees, and W. C. Johnson, The Gibbs–Thomson equation for a spherical coherent precipitate with applications to nucleation, *Scripta Met.* **22**:293–298 (1988).
145. P. W. Voorhees and W. C. Johnson, Development of spatial correlations during diffusional late-stage phase transformations in stressed solids, *Phys. Rev. Lett.* **61**:2225–2228 (1988).
146. W. C. Johnson, Precipitate shape evolution under applied stress—thermodynamics and kinetics, *Metall. Trans. A* **18A**:233–247 (1987).
147. W. C. Johnson and P. W. Voorhees, Elastic interaction and stability of misfitting cuboidal inhomogeneities, *J. Appl. Phys.* **61**:1610–1619 (1987).
148. I. M. Kaganova and A. L. Roitburd, Equilibrium shape of an inclusion in a solid, *Sov. Phys. Dokl.* **32**:925–7 (1987).
149. S. Yoshida, M. Fukaya, and T. Miyazaki, *J. Japan Inst. Metals* **51**:18 (1987).
150. M. B. Berkenpas, W. C. Johnson, and D. E. Laughlin, The influence of applied stress on precipitate shape and stability, *J. Mater. Res.* **1**:635–645 (1986).
151. M. A. Grinfeld, Construction of a physically linear theory of coherent phase transformations, *Izv. A. N. SSSR Mekhanika Tverdogo Tela* **21(5)**:79–91 (1986); English translation in *Mechanics of Solids* **21**:84–96 (1986).
152. W. C. Johnson and J. J. D. Alexander, Interfacial conditions for thermomechanical equilibrium in two-phase crystals, *J. Appl. Phys.* **59**:2735–2746 (1986).
153. P. W. Voorhees and W. C. Johnson, Interfacial equilibrium during a first-order phase transformation in solids, *J. Chem. Phys.* **84**:5108–5121 (1986).
154. T. Miyazaki, K. Seki, M. Doi, and T. Kozakai, Stability bifurcation in the coarsening of precipitates in elastically constrained systems, *Mater. Sci. Eng.* **77**:125–132 (1986).
155. W. W. Mullins, The statistical self-similarity hypothesis in grain growth and particle coarsening, *J. Appl. Phys.* **59**:1341–1349 (1986).
156. A. L. Roitburd, Phase equilibrium in solids, *Soviet Phys. Solid State* **28**:1716–1718 (1986). (English translation of *Fiz. Tverd. Tela* **28**:3051–3054).
157. J. B. Walsh, An introduction to stochastic partial differential equations, *École d'été de probabilités de St. Flour XIV*, P. L. Henneguin, ed., Lecture Notes Math 1180 (Springer, Berlin, 1986), pp. 265–437.
158. M. Doi, T. Miyazaki, and T. Wakatsuki, The effects of elastic interaction energy on the γ' precipitate morphology of continuously cooled nickel-base alloys, *Mater. Sci. Eng.* **74**:139–145 (1985).
159. H. Furukawa, *Adv. Phys.* **34**:703 (1985).
160. A. L. Roitburd, Thermodynamics of solid solution precipitation, *Sov. Phys. Solid State* **27**:982–90 (1985) (English translation of *Fiz. Tverd. Tela* **27**:982–90).
161. P. W. Voorhees, The theory of Ostwald ripening, *J. Stat. Phys.* **38**:231–252 (1985).
162. J. W. Cahn and F. C. Larché, A simple model for coherent equilibrium, *Acta Met.* **32**:1915–1923 (1984).

163. M. Doi, T. Miyazaki, and T. Wakatsuki, The effect of elastic interaction energy on the morphology of γ' precipitates in nickel-based alloys, *Mater. Sci and Eng.* **67**:247–253 (1984).
164. H. Furukawa, Dynamic scaling theory for phase-separating unmixing mixtures: growth rates of droplets and scaling properties of autocorrelation functions, *Physica A* **123**:497–515 (1984).
165. W. C. Johnson, On the elastic stabilization of precipitates against coarsening under applied load, *Acta Metall.* **32**:465–475 (1984).
166. W. C. Johnson and J. W. Cahn, Elastically induced shape bifurcations of inclusions, *Acta Metall.* **32**:1925–1933 (1984).
167. J. D. Gunton, M. San Miguel, and P. S. Sahni, The dynamics of first order phase transformations, *Phase Transitions and Critical Phenomena*, C. Domb and J. L. Lebowitz, eds., Vol. 8 (Academic Press, New York, 1983), pp. 267–466.
168. J. D. Gunton and M. Droz, *Introduction to the Theory of Metastable and Unstable States*, Lecture Notes in Physics, No. 183 (Springer-Verlag, 1983).
169. W. C. Johnson, Elastic interaction of two precipitates subjected to an applied stress, *Metall. Trans. A* **14A**:2219–2227 (1983).
170. A. G. Khachaturyan, *Theory of Structural Transformations in Solids* (Wiley, New York, 1983).
171. J. W. Morris, A. G. Khachaturyan, and S. H. Wen, The elastic contribution to the thermodynamics of phase transitions in solids, *Proceedings of the International Conference on Solid–Solid Phase Tranformations Held at Pittsburgh, Pa, August 1981* (cited by Khachaturyan[170]).
172. J. W. Cahn and F. C. Larché, Surface stress and the chemical equilibrium of single crystals. II. Solid particles imbedded in a solid matrix, *Acta Metall.* **30**:51–56 (1982).
173. F. C. Larché and J. W. Cahn, The effect of self-stress on diffusion in solids, *Acta Metall.* **30**:1835–1845 (1982).
174. T. Miyazaki, H. Imamura, and T. Kozakai, The formation of "γ' precipitate doublets" in Ni-Al alloys and their energetic stability, *Mat. Sci Eng.* **54**:9–15 (1982).
175. T. Mura, *Micromechanics of Defects in Solids* (Martinus Nijhoff, the Hague, 1982).
176. S. Wen, E. Kostlan, M. Hong, A. Khachaturyan, and J. W. Morris, The preferred habit of a tetragonal inclusion in a cubic matrix, *Acta Met.* **29**:1247–1254 (1981).
177. H. Zabel and H. Peisl, Coherent $\alpha - \alpha'$ phase transition of hydrogen in niobium, *Acta Met.* **28**:589–599 (1980).
178. S. M. Allen and J. W. Cahn, A microscopic theory for antiphase boundary motion and its application to antiphase domain coarsening, *Acta Metall.* **27**:1085–1095 (1979).
179. W. C. Johnson and J. K. Lee, Elastic interaction energy of two spherical precipitates in an anisotropic matrix, *Metal. Trans. A* **10A**:1141–1149 (1979).
180. T. Miyazaki, K. Nakamura, and H. Mori, Experimental and theoretical investigations on morphological changes of γ-precipitates in Ni-Al single crystals during uniaxial stress annealing, *J. Mater. Sci.* **14**:1827–1837 (1979).
181. V. Perovic, G. R. Purdy, and L. M. Brown, *Acta Met.* **27**:1075–1084 (1979).
182. H. Zabel and H. Peisl, Sample-shape-dependent phase transion of hydrogen in niobium, *Phys. Rev. Lett.* **42**:511–514 (1979).
183. F. C. Larché and J. W. Cahn, A nonlinear theory of thermochemical equilibrium of solids under stress, *Acta Metall.* **26**:53-60 (1978).
184. F. C. Larché and J. W. Cahn, Thermochemical equilibrium of multiphase solids under stress, *Acta Metall.* **26**:1579–1589 (1978).
185. J. K. Lee and W. C. Johnson, *Phys. Status Solidi* **46**:267 (1978).
186. E. Seitz and D. de Fontaine, Elastic interaction energy calculations for Guinier–Preston zones in Al-Cu and Cu-Be, *Acta Metall.* **26**:1671–1679 (1978).

187. J. K. Lee, D. M. Barnett, and H. I. Aaronson, The elastic strain energy of coherent ellipsoidal precipitates in anisotropic crystalline solids, *Metall. Trans.* **8A**:963–973 (1977).
188. A. Pineau, Influence of uniaxial stress on the morphology of coherent precipitates during coarsening—Elastic energy considerations, *Acta Metall.* **24**:559 (1976).
189. A. L. Roitburd and N. S. Kosenko, Elastic energy of a plate inclusion in an anisotropic elastic medium, *Scripta Met.* **11**:1039–1043 (1977).
190. J. D. Eshelby, The elastic energy-momentum tensor, *J. Elasticity* **5**:321–336 (1975).
191. M. E. Gurtin and I. Murdoch, A continuum theory of elastic material surfaces, *Arch. Rat. Mech. Anal.* **57**:291–323 (1975).
192. K. Binder, Kinetic Ising model study of phase separation in binary alloys, *Z. Phys.* **267**:313–322 (1974).
193. J. W. Cahn and D. W. Hoffman, A vector thermodynamics for anisotropic surfaces. II. Curved and faceted surfaces, *Acta Metall.* **22**:1205–1214 (1974).
194. W. G. Hoover, W. T. Ashurst, and R. J. Olness, Two-dimensional computer studies of crystal stability and fluid viscosity, *J. Chem. Phys.* **60**:4043–4047 (1974).
195. A. G. Khachaturyan and V. N. Airapetyan, Spatially periodic distributions of new-phase inclusions caused by elastic distortions, *Phys. Status Solidi* (*A*) **26**:61–70 (1974).
196. P. Y. Robin, Thermodynamic equilibrium across a coherent interface in a stressed crystal, *Amer. Mineralogist* **59**:1286–1298 (1974).
197. A. G. Khachaturyan and V. N. Hairapetyan, *Phys Status Solidi* (*B*) **35**:735 (1973) (cited by Khachaturyan[170]).
198. F. C. Larché and J. W. Cahn, A linear theory of thermomechanical equilibrium of solids under stress, *Acta Metall.* **21**:1051–1063 (1973).
199. D. De Fontaine, Analysis of clustering and ordering in multicomponent solid solutions I. stability criteria, *J. Phys. Chem. Solids* **33**:297–310 (1972).
200. M. E. Gurtin, *The Linear Theory of Elasticity* Handbuch der Physik VIa/2 1-295 (Springer-Verlag, Berlin, 1972).
201. H. E. Cook and D. de Fontaine, On the elastic energy of solid solutions II. influence of the effective modulus on precipitation from solution and the order–disorder reaction, *Acta Metall.* **19**:607–616 (1971).
202. J. K. Tien and S. M. Copley, The effect of uniaxial stress on the periodic morphology of coherent gamma prime precipitates in nickel-base superalloy crystals, *Metall. Trans.* **2**:215 (1971).
203. H. E. Cook, D. de Fontaine, and J. E. Hilliard, A model for diffusion on cubic lattices and its application to the early stages of ordering, *Acta Met.* **17**:765–773 (1969).
204. H. E. Cook, The kinetics of clustering and short-range order in stable solid solutions, *J. Phys. Chem Solids* **30**:2427–2437 (1969).
205. H. E. Cook and D. DeFontaine, On the elastic free energy of solid solutions—I. Microscopic theory, *Acta Metall.* **17**:915–924 (1969).
206. J. D. Eshelby, *Inelastic Behaviour of Solids*, M. F. Kanninen *et al.*, eds. (McGraw-Hill, New York, 1969), p. 77.
207. A. G. Khachaturyan, *Phys. Status Solidi* **35**:119 (1969).
208. A. G. Khachaturyan and G. A. Shatalov, Potential of elastic interaction of defects in a crystal, *Sov. Phys. Solid State* **11**:118 (1969) (English translation of *Fiz. Tverd. Tela* **11(1)**:59–66).
209. A. G. Khachaturyan and G. A. Shatalov, *Sov. Phys. JETP* **29**:557 (1969).
210. C. P. Sullivan, B. J. Piearcey, and G. A. Webster, *J. Inst. Metals* **96**:274 (1968).
211. A. Khachaturyan, *Sov. Phys. Solid State* **9**:2040 (1968) (English translation of *Fiz. Tverd. Tela* **9**:2595).

212. A. L. Roitburd, Orientational and habit relationships between crystalline phases in solid-state transformations, *Sov. Phys. Cryst.* **12**:499 (1968) (English translation of *Kristallografi* **12**:567–574 (1967)).
213. G. A. Webster and C. P. Sullivan, Some effects of temperature cycling on the creep behaviour of a nickel-base alloy, *J. Inst. Met.* **95**:138–142 (1967).
214. J. D. Eshelby, On the elastic interaction between inclusions, *Acta Met.* **14**:1306–1309 (1966) (appendix to A. J. Ardell, R. B. Nicholson, and J. D. Eshelby (1966) On modulated structure of aged Ni-Al alloys, *Acta Metall.* **14**:1295–1309).
215. A. G. Khachaturyan, Some questions concerning the theory of phase transitions in solids, *Fiz. Tverd. Tela.* **8**:2709–2717 (1966). English translation in *Sov. Phys. Solid. State* **8**:2163 (1966).
216. J. W. Cahn, (unpublished, circa 1964). Report 64-RL-356 M, General Electric Research laboratory, Schenectady, New York (cited by Thompson and Voorhees[26]).
217. A. G. Khachaturyan, Nonlinear integral equations and their application to the problem of orderable alloys (in Russian) *Fiz. Tverd. Tela* **5**:26–35 (1963). English translation: *Soviet Physics Solid State* **5**:16 (1963).
218. A. G. Khachaturyan, Nonlinear equations of integral type and their application to the study of the crystal symmetries of interstitial solutions (in Russian), *Fiz. Tverd. Tela* **5**:750–758 (1963). English translation: *Sov. Phys. Solid State* **5**:548–553.
219. W. W. Mullins and R. F. Sekerka, Morphological stability of a particle growing by diffusion or heat flow, *J. Appl. Phys.* **34**:323 (1963).
220. J. W. Cahn, On spinodal decomposition in cubic crystals, *Acta Metall.* **10**:179–183 (1962).
221. A. G. Khachaturyan, Application of the method of two-time Green's functions to the problem of ordering alloys (in Russian), *Fiz. Met. Metallogr.* **13**:493–501 (1962). English translation: *Physics of Metals and Metallography* **13(4)**:12–20.
222. J. W. Cahn, On spinodal decomposition, *Acta Metall.* **9**:795–801 (1961).
223. J. D. Eshelby, Elastic inclusions and inhomogeneities, *Prog. Solid Mech.* **2**:89–140 (1961).
224. M. Hillert, A solid solution model for inhomogeneous systems, *Acta Met.* **9**:525–535 (1961).
225. I. M. Lifshitz and V. V. Slyozov, The kinetics of precipitation from supersaturated solid solutions, *J. Phys. Chem. Solids* **19**:35–50 (1961).
226. C. Wagner, Theorie der Alterung von Niederschlägen durch Umlösung—Ostwald–Reifung, *Z. Electrochem.* **65**:581–591.
227. J. D. Eshelby, The elastic field outside an ellipsoidal inclusion, *Proc. Roy Soc. A* **252**:561–569 (1959).
228. L. D. Landau and E. M. Lifshitz, *Theory of Elasticity* (Pergamon, London, 1959). (English Translation by J B. Sykes and W. H. Reid of *Teoriya Uprugosti*, Izdat. "Nauka," Moscow).
229. J. D. Eshelby, The determination of the elastic field of an ellipsoidal inclusion, and related problems, *Proc. Roy. Soc. A* **241**:376–396 (1957).
230. W. W. Mullins, Theory of thermal grooving, *J. Appl. Phys.* **28**:333–339 (1957).
231. J. D. Eshelby, The continuum theory of lattice defects, *Solid State Physics* **3**:79–144 (1956).
232. M. Born and K. Huang, *Dynamical Theory of Crystal Lattices* (Oxford Univ. Press, Oxford, 1954).
233. J. D. Eshelby, The force on an elastic singularity, *Phil. Trans. Roy. Soc. Lond. A* **244**:87–112 (1951).
234. K. Robinson, Elastic energy of an ellipsoidal inclusion in an infinite solid, *J. Appl. Phys.* **22**:1045–1054 (1951).

235. M. M. Crum, Private communication cited in F. R. N. Nabarro (1940); The strains produced by precipitation in alloys, *Proc. Roy. Soc. A* **125**:519–538 (1940).
236. F. Bitter, On impurities in metals, *Phys Rev.* **37**:1527–1547 (1931).
237. J. D. van der Waals, The thermodynamic theory of capillarity under the hypothesis of a continuous variation of density (in Dutch), *Verhandel. Konink. Akad. Weten. Amsterdam* (Sect. 1), Vol. 1, No. 8 (1893). English translation by J. S. Rowlinson, *J. Stat. Phys.* **20**:197–244 (1979).